



doi:10.1016/S0016-7037(03)00140-6

The Geysers - Cobb Mountain Magma System, California (Part 1): U-Pb zircon ages of volcanic rocks, conditions of zircon crystallization and magma residence times

AXEL K. SCHMITT,^{1,*} MARTY GROVE,¹ T. MARK HARRISON,^{1,2} OSCAR LOVERA,¹ JEFFREY HULEN,³ and MARK WALTERS⁴¹Department of Earth and Space Sciences, University of California, Los Angeles, 595 Charles Young Dr. E, Los Angeles CA 90095-1567, USA²Research School of Earth Sciences, The Australian National University, Canberra, A.C.T. 0200, Australia³Energy and Geoscience Institute, University of Utah, 423 Wakara Way, Salt Lake City, UT 84108-1210, USA⁴Consulting Geologist, 1573 Manzanita Ave., Santa Rosa, CA 95404, USA

(Received July 2, 2002; accepted in revised form February 6, 2003)

Abstract—Combined U-Pb zircon and $^{40}\text{Ar}/^{39}\text{Ar}$ sanidine data from volcanic rocks within or adjacent to the Geysers geothermal reservoir constrain the timing of episodic eruption events and the pre-eruptive magma history. Zircon U-Pb concordia intercept model ages (corrected for initial ^{230}Th disequilibrium) decrease as predicted from stratigraphic and regional geological relationships (1σ analytical error): 2.47 \pm 0.04 Ma (rhyolite of Pine Mountain), 1.38 \pm 0.01 Ma (rhyolite of Alder Creek), 1.33 \pm 0.04 Ma (rhyodacite of Cobb Mountain), 1.27 \pm 0.03 Ma (dacite of Cobb Valley), and 0.94 \pm 0.01 Ma (dacite of Tyler Valley). A significant (\sim 0.2–0.3 Ma) difference between these ages and sanidine $^{40}\text{Ar}/^{39}\text{Ar}$ ages measured for the same samples demonstrates that zircon crystallized well before eruption. Zircons U-Pb ages from the underlying main-phase Geysers Plutonic Complex (GPC) are indistinguishable from those of the Cobb Mountain volcanics. While this is in line with compositional evidence that the GPC fed the Cobb Mountain eruptions, the volcanic units conspicuously lack older (\sim 1.8 Ma) zircons from the shallowest part of the GPC. Discontinuous zircon age populations and compositional relationships in the volcanic and plutonic samples are incompatible with zircon residing in a single long-lived upper crustal magma chamber. Instead we favor a model in which zircons were recycled by remelting of just-solidified rocks during episodic injection of more mafic magmas. This is consistent with thermochronologic evidence that the GPC cooled below 350° C at the time the Cobb Mountain volcanics were erupted. Copyright © 2003 Elsevier Ltd

1. INTRODUCTION

The issue of whether silicic magma chambers can remain viable in the upper levels of the continental crust for long durations is a matter of ongoing debate (e.g., Huppert and Sparks, 1988; Halliday et al., 1989). Recent ion microprobe study of zircon from Quaternary volcanic rocks (e.g., Reid et al., 1997; Brown and Fletcher, 1999; Reid and Coath, 2000; Bindeman et al., 2001; Vazquez and Reid, 2002) has highlighted the potential of this technique for assessing the longevity of large silicic magma systems. The sluggish diffusivity of U, Th, and Pb in zircon at magmatic temperatures (Watson et al., 1997; Cherniak and Watson, 2001) coupled with the propensity of zircon to dissolve rapidly in hydrous silicic melts at temperatures above zircon saturation (Harrison and Watson, 1983; Baker et al., 2002) give rise to the expectation that zircon U-Pb ages can record the onset of zircon crystallization in the magma (Reid et al., 1997). In contrast, $^{40}\text{Ar}/^{39}\text{Ar}$ ages of sanidine are conventionally expected to date the time of eruption (McDougall and Harrison, 1999). Measured discrepancies between zircon crystallization and eruption ages (e.g., Reid et al., 1997; Brown and Fletcher, 1999; Reid and Coath, 2000; Bindeman et al., 2001; Vazquez and Reid, 2002) may thus have the potential to provide an estimate for zircon residence time in magmas (e.g., Reid et al., 1997) or, alternatively, detect crystal recycling from earlier intrusions (e.g., Bindeman et al., 2001).

These contrasting conclusions bear directly on the nature and time scales of magma chamber processes.

The Geysers geothermal area in Northern California (Fig. 1) is an outstanding, economically important example of a long-lived, silicic magma-driven, geothermal system. Volcanic rocks erupted from Cobb Mountain directly over the eastern flank of a subsurface plutonic body, the Geysers Plutonic Complex (GPC) that underlies the area of highest heat flow within the Clear Lake region (Schriener and Suemnicht, 1981). Despite the evidence for plutonic rocks in the GPC being as old as \sim 1.8 Ma (see the Schmitt et al. companion paper in this issue), hydrothermal activity in the Geysers persisted in some form to the present day (e.g., Donnelly-Nolan et al., 1981; Dalrymple, 1993; Hulen et al., 1997; Dalrymple et al., 1999). Models explaining the current high heat flow of the Geysers - Clear Lake region (Fig. 1; Walters and Combs, 1992) invoke either a very large, continuously viable, mid to deep crustal magma body (Isherwood, 1981; McLaughlin, 1981) or transient heating produced by episodic near-surface intrusions (McLaughlin et al., 1983; Williams et al., 1993; Kennedy and Truesdell, 1996; Stanley et al., 1998; Stimac et al., 2001).

By studying volcanic rocks from Cobb Mountain and two additional centers positioned at either end of the northwest-southeast trending GPC (Pine Mountain and Tyler Valley; see Fig. 2) we have (1) documented the physical conditions attending zircon growth through the analysis of major and trace elemental compositional data from zircon crystals, melt inclusions, and whole rock samples; (2) measured zircon U-Pb ages throughout the volcanic section that significantly predate newly obtained eruption ages for the same samples; and (3) assessed

* Author to whom correspondence should be addressed (axel@argon.ess.ucla.edu).

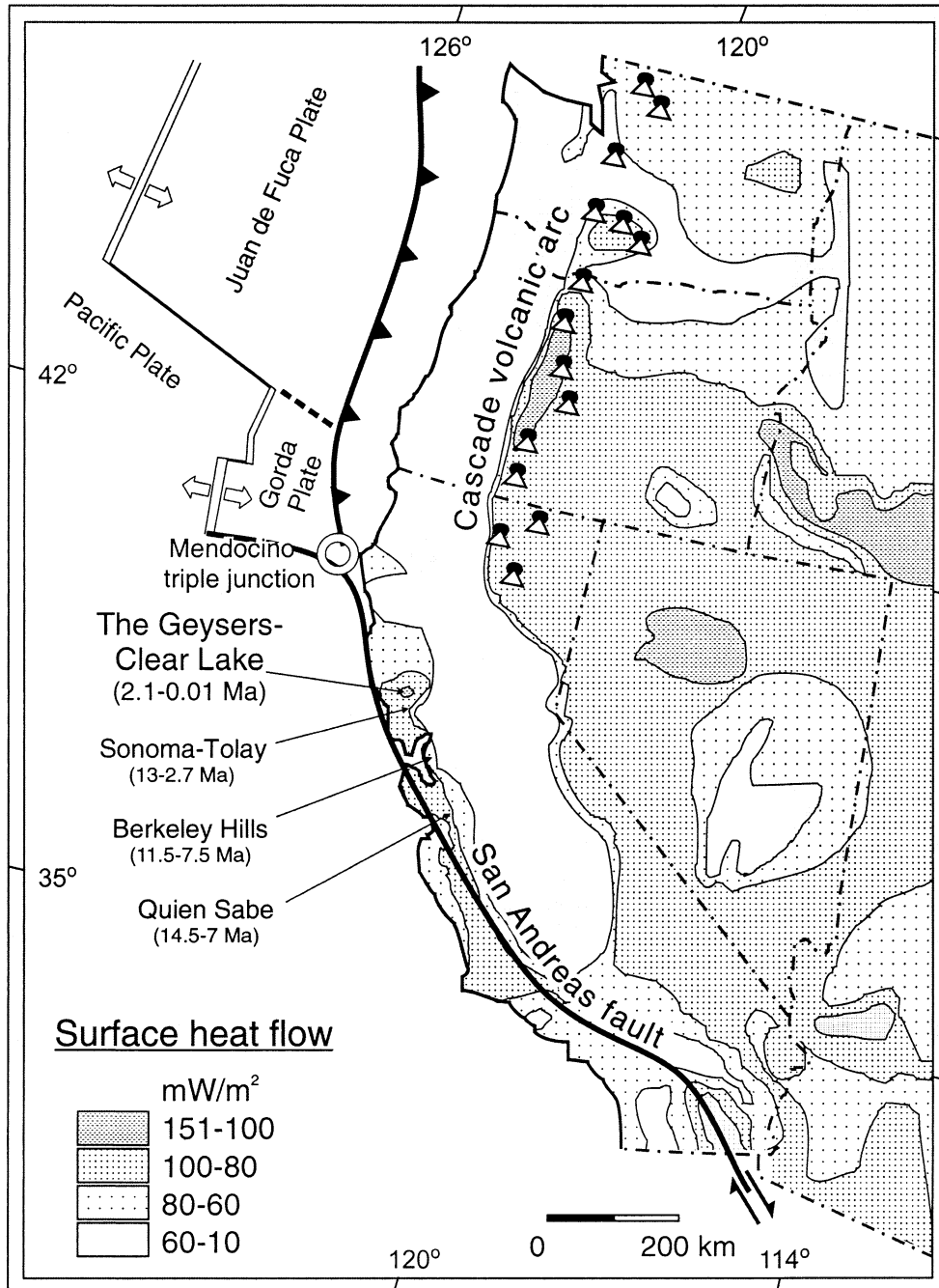


Fig. 1. Tectonic and heat flow map of the Western U. S. A. (modified after Dickinson and Snyder, 1979; Johnson and O'Neil, 1984; Blackwell and Steele, 1992) showing location of the Clear Lake volcanic field and age range of Coast Range volcanic centers. Note northward decrease in ages. Cascade volcanic arc volcanoes (triangles) shown for comparison (after Borg and Clynne, 1998).

the zircon crystallization and residence history and the implications for the nature and longevity of the Geysers – Cobb Mountain magma system. While the crystallization interval for the zircons from Cobb Mountain is in excellent agreement with the main (~1.2–1.4 Ma) intrusive phases within the GPC, the volcanic rocks contain no crystal record of the earliest ~1.8 Ma intrusion (Schmitt et al., this issue). Our results suggest that both the GPC and spatially related eruptives from the Pine

Mountain, Cobb Mountain, and Tyler Valley centers were fed by discrete batches of magma. Comparison with previously determined thermal histories for the GPC (Dalrymple et al., 1999) leads us to conclude that the older zircon U-Pb crystallization ages (relative to ⁴⁰Ar/³⁹Ar eruption ages) in the Cobb Mountain volcanics do not result from protracted magma storage in a single, long-lived (>0.2 Ma) shallow magma chamber. We instead propose that these differences are best explained by

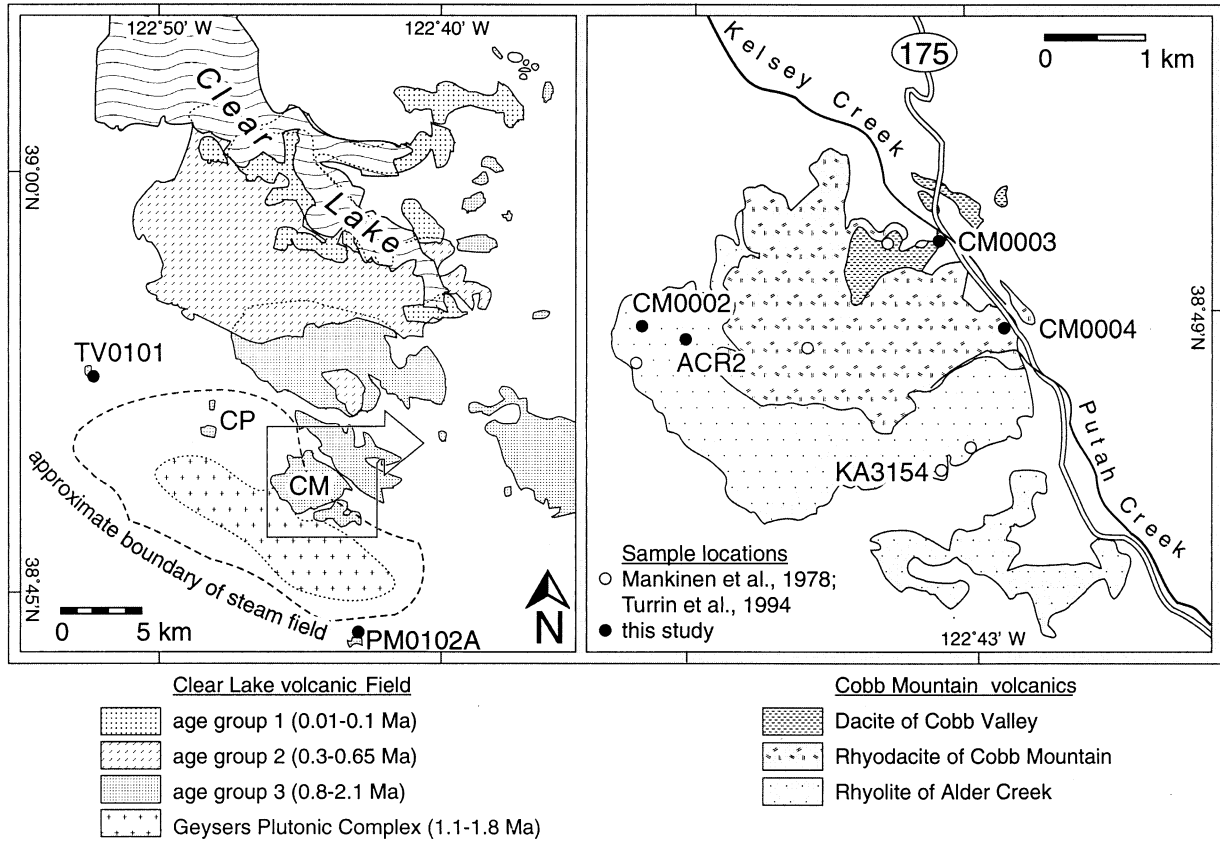


Fig. 2. Eastern Coast Range volcanic fields including the Clear Lake volcanic field and the Geysers - Cobb Mountain centers. Outline of the subsurface extent of the hypabyssal Geysers plutonic complex (GPC) projected from -3000 m below sea-level (mbsl). Sample locations for $^{40}\text{Ar}/^{39}\text{Ar}$ and U-Pb dating are indicated. Abbreviations: TV = Tyler Valley; CP = Caldwell Pines; CM = Cobb Mountain; PM = Pine Mountain; Sample location KA3154 from Turrin et al. (1994).

remelting portions of the just-emplaced, and rapidly cooled, GPC in response to episodic magma influx.

2. GEOLOGICAL BACKGROUND

2.1. Northeastern Coast Range Magmatism

Volcanic rocks in the Geysers - Cobb Mountain area are part of the late-Pliocene-Holocene Clear Lake volcanic field that occurs within the eastern Coast Range of northern California, east of the San Andreas fault and southwest of the active Cascade magmatic arc (Fig. 1; Hearn et al., 1981, 1995). This field is the youngest in a series of Middle Tertiary to Quaternary volcanic centers that were established after northwestward migration of the Mendocino triple junction (Fig. 1; Dickinson and Snyder, 1979; Johnson and O'Neil, 1984; Fox et al., 1985). Northeastern Coast Range volcanism has been interpreted of being generated above an area of asthenospheric upwelling and basalt generation in the slab-free window that is formed immediately east of the San Andreas transform as subduction ceases (Dickinson and Snyder, 1979; Lachenbruch and Sass, 1980; Liu and Furlong, 1992; Liu, 1993; Goes et al., 1997; Levander et al., 1998; Stimac et al., 2001). Geophysical measurements are consistent with anatexis of the lower crust (i.e., below ~ 15 km depth) in response to basaltic underplating (Stanley et al.,

1998). The presence of magma at shallow crustal levels (< 7 km) has been argued for on the basis of seismic imaging (Iyer et al., 1981; Eberhart-Phillips, 1986; Benz et al., 1992; Stanley and Blakely, 1995).

Oxygen and strontium isotopic data for the dominantly intermediate to felsic northeastern Coast Range volcanic rocks indicate of a significant crustal component (Johnson and O'Neil, 1984). Consequently, petrogenetic models of Clear Lake volcanism invoked episodic basaltic intrusions into the crust that trigger crustal melting and the production of dominantly rhyolitic magmas that were followed by smaller volumes of (rhyo-)dacitic compositions (Donnelly-Nolan et al., 1981). Futa et al. (1981) reported feldspar and whole-rock Sr abundances and $^{87}\text{Sr}/^{86}\text{Sr}$ ratios from Clear Lake samples that include Cobb Mountain rocks to be out of equilibrium as a result of magma mixing. This interpretation is consistent with ubiquitous mafic mineral aggregates and disequilibrium textures present in Clear Lake volcanic rocks (A. Stimac, personal communication).

2.2. Pine Mountain, Cobb Mountain, and Tyler Valley Volcanics

The Pine Mountain, Cobb Mountain, and Tyler Valley centers comprise the southwesternmost and oldest part in the Clear

Table 1. Results of previous K-Ar ($^{40}\text{Ar}/^{39}\text{Ar}$) age determinations for Geysers - Cobb Mountain volcanic rocks (sanidine and whole-rock) and new $^{40}\text{Ar}/^{39}\text{Ar}$ sanidine results (this study)

Sample	Unit	Longitude W	Latitude N	Literature age [Ma] ^a		Reference ^b	$^{40}\text{Ar}/^{39}\text{Ar}$ age ^c		MSWD	n ^d
					$\pm 1 \sigma$		[Ma]	$\pm 1 \sigma$		
Pine Mountain PM-01-02A	Rhyolite of Pine Mountain	122.6950	38.7334	2.06	0.02	1	2.17	0.02	1.6	12
Cobb Mountain KA3154	Rhyolite of Alder Creek	122.7200	38.8017	1.19*	0.01	2	1.16	0.02	0.63	22
CM0002	Rhyolite of Alder Creek	122.7667	38.8137				1.15	0.02	0.21	14
all ACR	Rhyolite of Alder Creek						1.15	0.01	0.45	36
CM0004	Rhyodacite of Cobb Mountain	122.7125	38.8158	1.06	0.02	1	1.10	0.02	0.20	11
CM0003	Dacite of Cobb Valley	122.7213	38.8237	1.08	0.02	1	1.00	0.05	0.34	10
Tyler Valley TV-01-01	Dacite of Tyler Valley	122.9014	38.8714	0.82	0.02	1	0.67	0.01	0.27	13

^a K/Ar or $^{40}\text{Ar}/^{39}\text{Ar}$ (*) age.

^b 1 Donnelly-Nolan et al. (1981); 2 Turrin et al. (1994).

^c weighted average age; analytical errors only.

^d n = numbers of averaged laser total fusion experiments; each experiment comprised 5-10 individual 250–350 μm sanidine grains.

Lake Volcanic field (Donnelly-Nolan et al., 1981). They occur in a NW-SE array that parallels the underlying GPC ($>300 \text{ km}^3$) and associated steam field (Fig. 2). Intermediate to felsic volcanic rocks erupted from central vent locations through metagreywacke and serpentinite of the Mesozoic Franciscan subduction complex (McLaughlin, 1981). The largest center among them, Cobb Mountain, is about 5 km in diameter (Fig. 2) and comprises a total $\sim 5 \text{ km}^3$ of erupted materials in three units (Hearn et al., 1995). Outcrops of rhyolite of Pine Mountain and dacite of Tyler Valley flows are much smaller in volume (0.02 km^3 and 0.003 km^3 respectively; Hearn et al., 1995).

The rhyolitic units (rhyolite of Pine Mountain and rhyolite of Alder Creek - ACR) are typically crystal-rich ($\sim 30\%$; Hearn et al., 1995) with phenocrysts of quartz, plagioclase, sanidine and biotite in a highly devitrified perlitic matrix. (Rhyo-)dacitic and dacitic volcanic rocks range from coarsely (rhyodacite of Cobb Mountain - CMD) to moderately (dacite of Tyler Valley), and sparsely porphyritic (dacite of Cobb Valley - CVD). Plagioclase, quartz, sanidine and biotite are the main phenocryst phases, but pyroxene-rich mafic inclusions or their disintegrated remnants are present in all units. The Cobb Mountain suite (ACR, CMD, and CVD) is of particular interest because it directly overlies the eastern flank of the GPC and in part caps the host-rocks of the geothermal system. Thus, these rocks may represent the volcanic equivalent of the GPC plutonic rocks (Schriener and Suemnicht, 1981; Hulen and Nielson, 1993).

Table 1 summarizes results from previous geochronological studies for the selected units. Transitional paleomagnetic directions were recognized in Cobb Mountain rocks and later recognized as a worldwide event of normal magnetic polarity (Mankinen et al., 1978). As a result, it was designated as The Cobb Mountain Normal Polarity Subchron and correlated with a 1.19 Ma age of the astronomical polarity time scale (Shackleton et al., 1990; Turrin et al., 1994). While intermediate to felsic compositions volumetrically dominate in the southwestern Clear Lake area, it is important to note that olivine basalt intermittently erupted at $1.66 \pm 0.12 \text{ Ma}$ (Caldwell Pines location in Fig. 2; Donnelly-Nolan et al., 1981).

3. MATERIAL AND METHODS

3.1. Sampling

Locations of the samples studied are shown in Table 1 and Figure 2. We also included in our analysis an additional sample of ACR (KA3154) that had been previously analyzed by K-Ar (Mankinen et al., 1978) and $^{40}\text{Ar}/^{39}\text{Ar}$ (Turrin et al., 1994) methods. Samples comprised 2–3 kg of rock from which aliquots were obtained for thin section preparation, mineral separation and whole-rock geochemical analysis. Mineral grains for dating and melt inclusion studies were concentrated from crushed and sieved materials. Following heavy-liquid and/or magnetic separation, sanidine and zircon crystals were hand selected with the aid of a binocular microscope.

3.2. Melt Inclusion, Mineral and Whole-Rock Geochemistry

Whole-rock analysis was performed with finely crushed ($<63 \mu\text{m}$) aliquots of the samples. Major and trace elements were determined by X-ray fluorescence analysis at the GeoForschungsZentrum Potsdam. Nb, Th and U were determined by inductively-coupled plasma mass spectrometry (ICP-MS) also at the GeoForschungsZentrum Potsdam.

Melt inclusions were studied in hand-selected quartz grains from ACR that were between 1.6–0.6 mm in diameter. To homogenize devitrified regions, quartz grains with sufficiently large inclusions ($>50 \mu\text{m}$ in diameter) were heated for 48 h in a pressurized vessel. Two sets of quartz crystals were run at temperatures of 850°C and 900°C, respectively. After quenching, most inclusions appeared glassy with a gas bubble typically present. Individual crystals were mounted in Araldite® epoxy and melt inclusions were exposed by grinding and polishing with Al_2O_3 (0.3 μm final polishing). We used Fourier transformed infrared spectroscopy methods (FTIR; Ihinger et al., 1994; Zhang et al., 1999) for reconnaissance H_2O and CO_2 measurements.

Major element compositions for melt inclusions and feldspar separates were obtained using a fully automated CAMECA

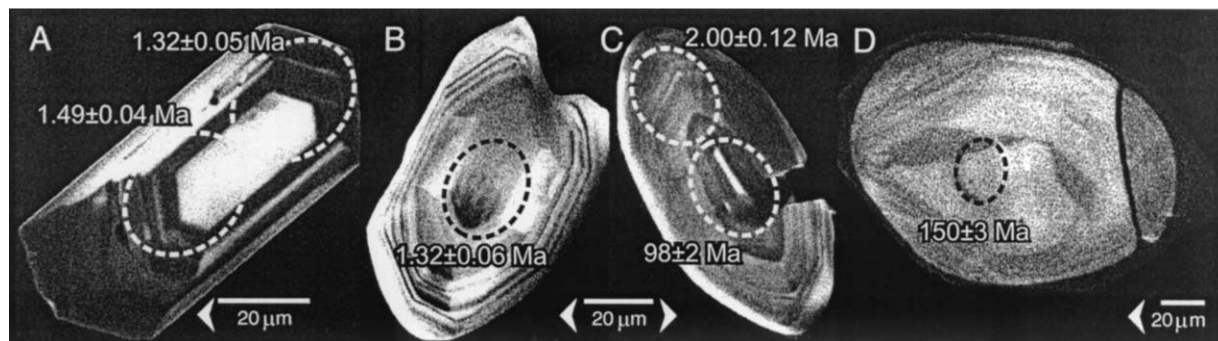


Fig. 3. Selected cathodoluminescence images of zircon from Cobb Mountain samples. a) rhyolite of Alder Creek CM0002 g13; b) dacite of Cobb Valley CM0003 g15; c) dacite of Cobb Valley CM0003 g6; d) rhyolite of Alder Creek CM0002 g6. Note rounded outer crystal boundaries in b and c and rounded core with euhedral overgrowth in c and d.

SX100 at the GeoForschungsZentrum Potsdam. X-rays were excited with 15 kV accelerating potential and a 10 nA beam. To minimize Na loss during glass analysis, the beam was rastered over a $20 \mu\text{m}^2$ area.

Trace element compositions of melt inclusion glasses were measured using the UCLA CAMECA ims 1270 ion probe. A ~ 1 nA primary mass-filtered $^{16}\text{O}^-$ beam was used at 22.5 keV impact energy. Positive secondary ions were extracted at 10 kV and analyzed at low mass resolution applying energy filtering in the range of -100 ± 25 eV to suppress molecular ion interferences on the analyzed masses ($^7\text{Li}^+$, $^8\text{Be}^+$, $^{11}\text{B}^+$, $^{30}\text{Si}^+$, $^{85}\text{Rb}^+$, $^{88}\text{Sr}^+$, $^{89}\text{Y}^+$, $^{90}\text{Zr}^+$, $^{93}\text{Nb}^+$, $^{138}\text{Ba}^+$, $^{139}\text{La}^+$, $^{140}\text{Ce}^+$, $^{232}\text{Th}^+$, $^{238}\text{U}^+$). Relative sensitivities of analyzed trace elements against $^{30}\text{Si}^+$ were calibrated on the NIST SRM 610 reference glass (Pearce et al., 1997). The standard error in trace element abundances of the melt inclusion glasses propagated from in-run precision and reproducibility of reference glass measurements typically ranges between $<5\%$ (Li, B, Rb, Sr, Ba, La), $<10\%$ (Y, Zr, Ce) and 20–40% (Nb, Th, U). Based on the agreement between measured values and reference values for natural and synthetic glasses, we estimate the accuracy of the melt inclusion analyses to be better than $\sim 25\%$.

3.3. $^{40}\text{Ar}/^{39}\text{Ar}$

Approximately 50 mg of sanidine from each sample was packed in Al-foil, sealed in quartz tubes under vacuum, and irradiated for 3 h in the unshielded 5C position of the McMaster reactor. Aliquots of Fish Canyon (FC) sanidine and salts (CaF_2 and K_2SO_4) were interspersed with the Cobb Mountain samples to determine irradiation and correction parameters. Argon liberated by fusing five to ten 250–350 μm grains with a 10 W CO_2 -laser was purified with a 50 L/s ST101 alloy SAES getter pump and analyzed with a VG 1200S mass spectrometer. Additional description of $^{40}\text{Ar}/^{39}\text{Ar}$ data reduction parameters is presented with data tables obtainable from http://oro.ess.ucla.edu/labdata/data_repository.html.

3.4. U-Th-Pb

Epoxy grain mounts of hand-selected zircons (from the $<250 \mu\text{m}$ fraction) were sectioned to expose grain interiors and polished with 1 μm Al_2O_3 . After ultrasonic cleaning, grains

were surveyed for internal compositional zonation and/or inclusions via cathodoluminescence (CL) imaging using a Leo 1430VP scanning electron microscope (Fig. 3). U-Pb ages were obtained using the UCLA CAMECA ims 1270 ion probe. Samples that had been coated with ~ 10 nm of Au were typically probed with a mass-filtered, 10–20 nA $^{16}\text{O}^-$ beam focused to a ~ 30 – $35 \mu\text{m}$ diameter spot. Secondary ions were extracted at 10 kV with an energy band-pass of 35 eV. The mass spectrometer was tuned to a mass resolution of ~ 5000 to resolve molecular interferences in the mass range analyzed ($^{94}\text{Zr}_2\text{O}^+$, $^{204}\text{Pb}^+$, $^{206}\text{Pb}^+$, $^{207}\text{Pb}^+$, $^{208}\text{Pb}^+$, $^{238}\text{U}^+$, $^{232}\text{Th}^{16}\text{O}^+$, $^{238}\text{U}^{16}\text{O}^+$). Pb^+ yields were increased by a factor of ~ 2 by flooding the analysis surface with O_2 at a pressure of $\sim 4 \times 10^{-3}$ Pa. The relative sensitivities for Pb and U were determined on reference zircon AS-3 (Paces and Miller, 1993) using a calibration technique similar to Compston et al. (1984). Th and U contents were estimated by multiplying measured $^{232}\text{Th}^{16}\text{O}^+ / ^{94}\text{Zr}_2\text{O}^+$ and $^{238}\text{U}^{16}\text{O}^+ / ^{94}\text{Zr}_2\text{O}^+$ ratios on the unknowns with corresponding relative sensitivity values determined on reference zircon 91500 (Th = 28.6 ppm; U = 81.2 ppm; Wiedenbeck et al., 1995).

Analysis surfaces were presputtered for 4 min before analysis to minimize surficial Pb contamination. Despite this, our results were still sensitive to common Pb derived from the more slowly sputtered crater margins. Although we found that more radiogenic Pb signals could be obtained by restricting the field aperture to only allow ions from the central portion of the crater to be transported into the mass spectrometer, overall intensities decreased significantly and compromise settings were required (see 4.3.4.).

4. RESULTS

4.1. Magma and Melt Composition

Whole-rock and melt inclusion compositional data for rocks from the Geysers - Cobb Mountain igneous complex are presented in Table 2 and Figure 4. Figure 4 shows the compositional range of GPC samples for comparison (Hulen and Nielson, 1993; this study). Note that surface and subsurface samples are compositionally very similar which led previous workers to suggest a close genetic link between the volcanic

Table 2. Major and trace element compositions for whole rocks for Geysers-Cobb Mountain volcanic rocks and selected Alder Creek rhyolite (ACR) melt inclusion glasses

Sample/well unit ^b type T _{hom} ^c	GDC21 ^a		CA5636 7 4F 21			CM0002											
	5865M	5865D	10500	11700	12900	1-Q5 MI1	1-Q8 MI1	1-Q9 MI1	2-Q1 MI1	2-Q2 MI1	2-Q3 MI1						
	microgranite porphyry		orthopyroxene-biotite granite			ACR											
	TVD	CVD	CM0004 CMD	CM0002 ACR	PM0102A PMR	w.r.	w.r.	w.r.	w.r.	w.r.	w.r.	glass 850°C	glass 850°C	glass 850°C	glass 900°C	glass 900°C	glass 900°C
[wt.%]																	
SiO ₂	66.1	66.8	67.4	72.3	73.6	71.9	73.0	78.6	76.3	76.0	77.4	72.5	75.1	70.7	75.6	74.0	
TiO ₂	0.53	0.57	0.67	0.17	0.34	0.26	0.26	0.13	0.14	0.26	0.06	0.05	0.08	0.16	0.09	0.08	
Al ₂ O ₃	16.9	16.8	16.8	13.0	15.0	14.5	15.0	11.5	11.1	11.9	12.4	15.6	13.7	16.6	13.8	14.8	
Fe ₂ O ₃	5.85	3.90	4.04	1.30	1.84	2.05	1.44	1.64	4.09	2.93	0.72	0.68	0.81	0.78	0.79	0.67	
MnO	0.08	0.06	0.07	0.02	0.01	0.03	0.02	0.02	0.29	0.07	0.03	b.d.	0.04	b.d.	0.06	0.10	
MgO	1.57	2.56	1.67	0.21	0.57	1.12	0.67	0.31	0.42	0.51	0.03	0.06	0.05	0.09	0.07	0.06	
CaO	2.80	2.83	2.87	0.81	1.25	1.87	2.14	1.01	1.71	1.43	0.35	0.73	0.48	0.85	0.56	0.72	
Na ₂ O	3.35	3.73	3.33	2.83	3.44	4.13	4.51	2.96	2.73	3.01	3.77	4.55	4.25	4.93	4.01	4.03	
K ₂ O	2.72	2.65	2.93	4.35	3.82	4.04	2.90	3.80	3.19	3.82	5.20	5.83	5.43	5.84	4.99	5.42	
P ₂ O ₅	0.12	0.14	0.15	0.03	0.09	0.15	0.13	0.04	0.05	0.08	b.d.	0.01	b.d.	0.03	b.d.	0.06	
total ^d	100.3	99.7	99.8	99.3	99.5	99.8	99.5	99.5	100.3	98.4	99.1	100.2	99.2	98.2	98.0	99.3	
[wt.%]																	
H ₂ O	1.19	1.36	1.68	1.02	0.95	0.48	0.46	0.34	3.48	0.55	1.38	2.03	2.12	–	–	–	
CO ₂	1.56	0.10	0.13	0.06	0.09	0.49	0.49	0.07	0.18	0.12	b.d.	b.d.	b.d.	–	–	–	
Cl	–	–	–	–	–	–	–	–	–	–	0.09	0.11	0.10	0.13	0.11	0.12	
[ppm]																	
Li	–	–	–	–	–	–	–	–	–	–	1699	1586	1586	1753	1303	1762	
Be	–	–	–	–	–	–	–	–	–	–	3.7	2.8	2.8	3.1	2.8	2.5	
B	–	–	–	–	–	–	–	–	–	–	288	259	259	261	215	201	
Rb	79	88	102	198	138	175	113	159	123	139	282	260	298	328	329	306	
Sr	520	379	319	79	109	123	147	100	111	143	4.6	32	19	26	15	31.9	
Y	19	64	23	21	19	41	27	23	17	22	18	3.6	16	28	23	18	
Zr	124	150	146	114	139	109	97	138	146	188	38	8.6	18	89	84	56	
Nb	–	6.7	8.0	6.9	–	–	–	5.0	5.9	6.0	4.8	1.5	4.6	15	10	8.3	
Ba	871	837	807	768	834	460	295	423	557	659	82	563	312	257	123	546	
La	–	–	–	–	–	–	–	–	–	–	18	9.5	19	32	26	22	
Ce	–	–	–	–	–	–	–	–	–	–	29	15	34	55	42	40	
Th	–	8.6	11	21	–	–	–	14	21	14	12	2.4	10	32	17	18	
U	–	3.7	4.4	7.5	–	–	–	4.2	8.0	3.8	5.0	2.6	3.2	9.0	8.0	10	

^a 5865M = matrix; 5865D = dike.

^b Abbreviations used: TVD = dacite of Tyler Valley; CVD = dacite of Cobb Valley; CMD = rhyodacite of Cobb Mountain; ACR = rhyolite of Alder Creek; PMR = rhyolite of Pine Mountain.

^c Temperature of rehomogenization (at 100 MPa; 48h).

^d Oxides normalized to 100% volatile-free. For glass analyses: includes direct measurement of oxygen.

w.r. whole-rock.

–not analyzed.

b.d. not detected.

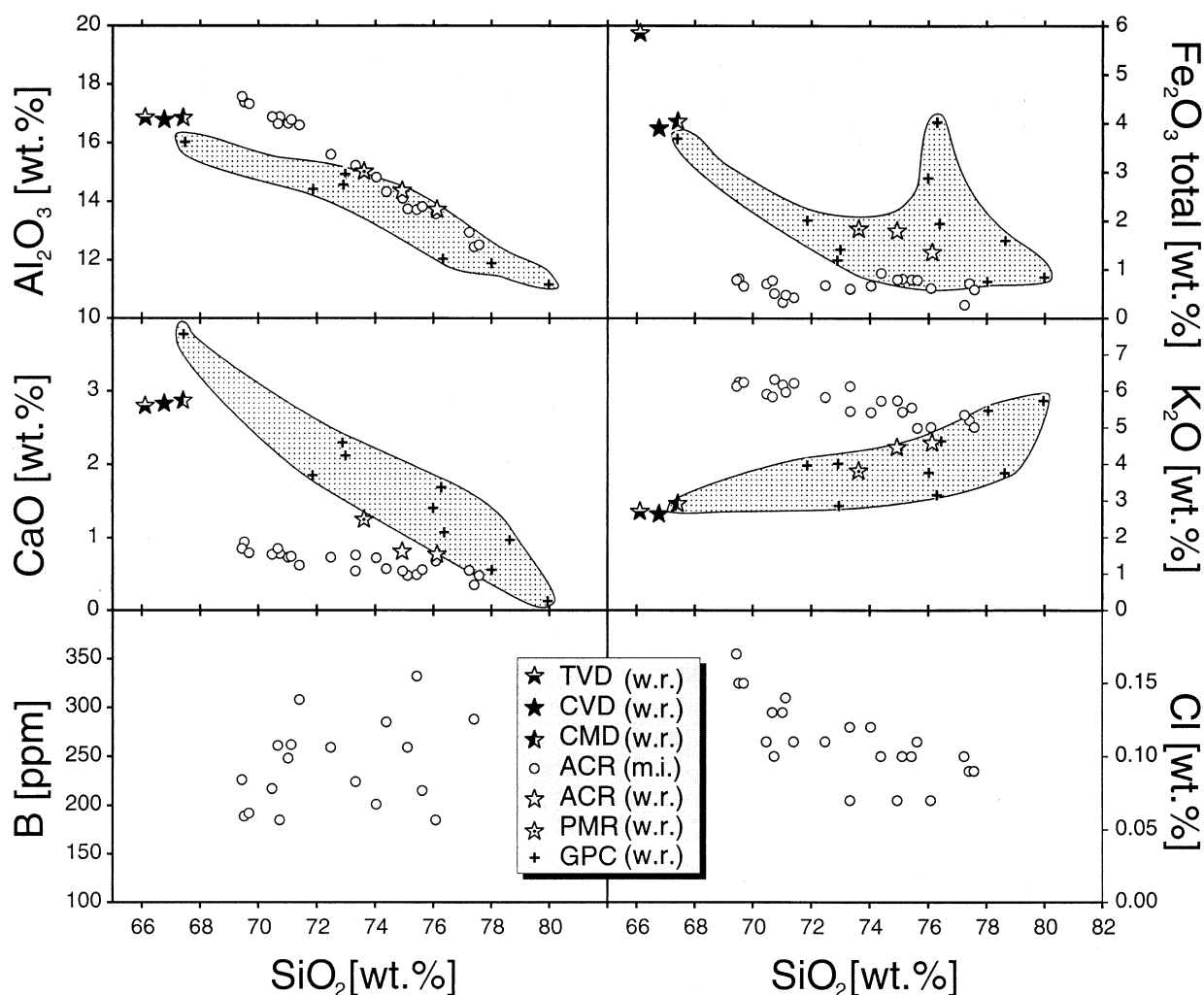


Fig. 4. Selected major and trace element variations against SiO_2 for the Geysers - Cobb Mountain whole-rock (w.r.) samples and melt inclusion glasses (m.i.). Whole-rock analyses were performed by X-ray fluorescence analysis (XRF). Melt inclusion glasses were analyzed by electron microprobe for major elements and Cl, and by secondary ion mass spectrometry (SIMS) for selected trace elements. Abbreviations used: TVD = dacite of Tyler Valley; CVD = dacite of Cobb Valley; CMD = rhyodacite of Cobb Mountain; ACR = rhyolite of Alder Creek; PMR = rhyolite of Pine Mountain; GPC = Geysers Plutonic complex (this study and Hulen and Nielson, 1993).

and plutonic units in the Geysers area (Schriener and Suemnicht, 1981; Hulen and Nielson, 1993).

Major and trace elements variations show systematic decrease of Al_2O_3 and CaO with increasing SiO_2 in a series of melt inclusions from the ACR (Fig. 4). The observed trends (e.g., $\text{CaO} \neq 0$ wt.% at 100 wt.% SiO_2) are inconsistent with postentrapment crystallization of quartz. Mixing between rhyodacitic and rhyolitic melts cannot explain the variations between low-Si and high-Si melt inclusion compositions since they fall off a potential mixing line between such end-members (Fig. 4). Hence, we interpret melt inclusion major element compositional trends to reflect variations in melt composition caused by crystallization of a dominantly quartzo-feldspathic mineral assemblage.

U and Th abundances in both the whole-rock and melt inclusion data define an enrichment line with a constant Th/U ratio of 2.3 (Fig. 5). Note that only the most evolved ACR melt

inclusion glasses have Th and U abundances close to or slightly higher than the whole rock compositions. High field strength elements (HFSE) like Y, Nb, Zr, La, Ce, Th and U typically show large variations in ACR melt inclusion glasses. Although we attempted to homogenize the inclusions by heating and quenching them before analysis, we at least in one case identified a small ($<1 \mu\text{m}$) crystallite as zircon. While additional undetected zircon crystallites (either incompletely dissolved during the homogenization process or precipitated during quenching) could be responsible for some of the observed scatter in Zr content, the overall variations of HFSE abundances are unlikely to be an experimental artifact. This is because of the strong correlations between trace elements that are not controlled by the presence of zircon. For example, both Nb and light REE such as La are expected to have low abundances in zircon (Hinton and Upton, 1991), but they are highly correlated with Zr in the melt inclusion glass analyses (Fig. 6).

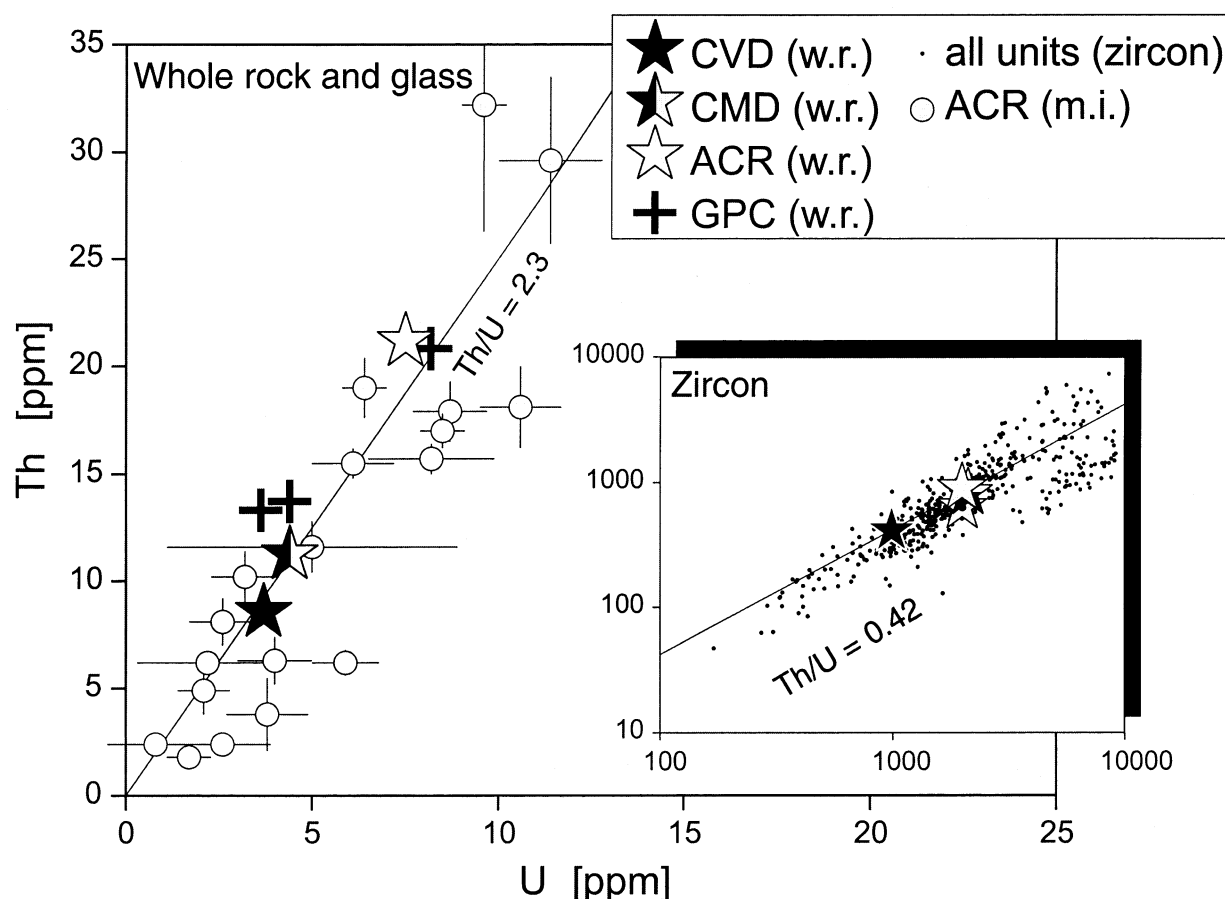


Fig. 5. Th vs. U in whole rock determined by inductively coupled plasma mass spectrometry (ICP-MS) and melt inclusion glasses (SIMS). Inset shows Th vs. U in volcanic and plutonic zircons (by SIMS; this study and Schmitt et al., this issue) and average compositions of the volcanic samples from the Geysers – Cobb Mountain. Reference lines for $\text{Th}/\text{U} = 2.3$ (whole rock and melt inclusion glasses) and $\text{Th}/\text{U} = 0.42$ (zircon) are drawn. Error bars are 1σ and symbols as in Fig. 4.

Rim compositions of feldspar phenocrysts (as indicated by remnants of adhering matrix glass) were analyzed to constrain preeruptive magma temperatures. Relatively constant feldspar compositions (e.g., average rim composition in ACR plagioclase $\text{An}_{0.23}\text{Ab}_{0.71}\text{Or}_{0.06}$ and sanidine $\text{An}_{0.01}\text{Ab}_{0.33}\text{Or}_{0.66}$; (unpublished data) and the scarcity of obvious disequilibrium textures such as sieved plagioclase allows preeruptive temperatures to be estimated for all samples except for CVD (CM0003). Two-feldspar thermometry using the calibration of Green and Usdansky (1986) yielded temperatures for the Ab, Or, and An calibrations that agree within $\pm 20^\circ\text{C}$ and range from $\sim 750\text{--}780^\circ\text{C}$ for rhyolites (ACR and Pine Mountain) and $\sim 790\text{--}820^\circ\text{C}$ for (rhyo-)dacites (CMD and Tyler Valley). CVD presumably was in compositional disequilibrium as indicated by plagioclase compositions ranging from $\text{An}_{0.62}\text{Ab}_{0.37}\text{Or}_{0.01}$ to $\text{An}_{0.22}\text{Ab}_{0.71}\text{Or}_{0.07}$ (unpublished data). Disequilibrium due to magma mixing and reheating is also supported by evidence for resorption in CVD zircons (Fig. 3b,c).

Zircon saturation temperatures (Watson and Harrison, 1983) calculated from whole-rock compositions fall within a narrow range for most of the Geysers - Cobb Mountain rhyolites and (rhyo-)dacites ($775\text{--}790^\circ\text{C}$; see Fig. 6); somewhat lower zir-

con saturation temperatures are found for the Tyler Valley sample ($\sim 750^\circ\text{C}$). In Figure 6 we also illustrated the range for plutonic rocks and note again a close similarity between volcanic and plutonic units. In contrast, zircon saturation temperatures calculated for the melt inclusion glasses span a wide range ($560\text{--}720^\circ\text{C}$) that is well below the values from two-feldspar thermometry (Fig. 6). The implications of this important observation are considered in the discussion.

A final point worth mentioning is that Cl and SiO_2 are inversely correlated, whereas B, a similarly incompatible trace element, remains approximately constant with increasing SiO_2 (Fig. 4). Similar observations elsewhere have been cited as evidence that a melt evolved under volatile saturated conditions (Stix and Layne, 1996). This occurs because B has a lower partitioning coefficient between melt and fluid compared to Cl (Pichavant, 1981; Webster and Holloway, 1988).

4.2. $^{40}\text{Ar}/^{39}\text{Ar}$

Tabulated $^{40}\text{Ar}/^{39}\text{Ar}$ results for all samples investigated are available from http://oro.ess.ucla.edu/labdata/data_repository.html. A summary of the results is provided in Table 1. Note

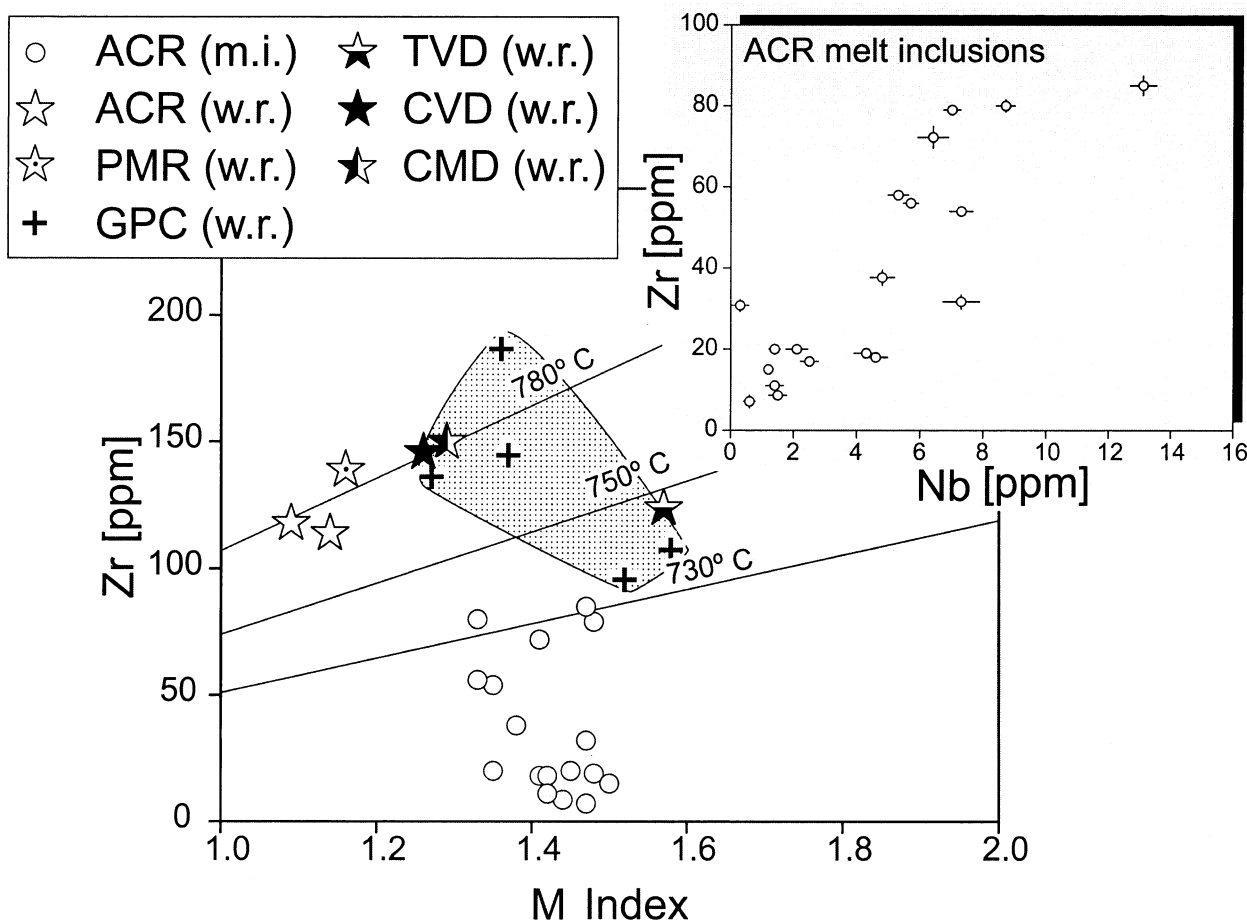


Fig. 6. Zr contents vs. M index defined as molar $(\text{Na}_2\text{O} + \text{K}_2\text{O} + 2\text{CaO}) / (\text{Al}_2\text{O}_3 + \text{SiO}_2)$ for the Geysers - Cobb Mountain whole-rock samples and melt inclusions glasses. Lines indicate zircon saturation isotherms calculated following Watson and Harrison (1983). Melt inclusion glasses yield unreasonably low apparent zircon saturation temperatures whereas whole-rock data overlap with preeruptive temperature estimates derived from two-feldspar thermometry ($\sim 780^\circ\text{C}$ for ACR). Note strong correlation between Zr and Nb for melt inclusion glasses shown in inset (error bars 1σ) that results from incompatible behavior of both, Zr and Nb. This implies that the melt at the time of inclusion entrapment was zircon undersaturated.

that the uncertainties listed in Table 1 are $\pm 1\sigma$ standard errors that reflect analytical uncertainties only. To maintain consistency with Turrin et al. (1994), we assigned our Fish Canyon (FC) sanidine flux monitors the 27.84 Ma age proposed by Cebula et al. (1986). Uncertainties in the K-Ar calibrations used to derive the ages of the standards employed as well as the decay constants ($\pm 1.0\%$; see Renne et al., 1998) cause the absolute errors associated with these results to be at least ± 0.02 Ma.

Both weighted average and inverse isochron $^{40}\text{Ar}/^{39}\text{Ar}$ ages decrease in accordance to stratigraphic order. The rhyolite of Alder Creek is the oldest unit in the Cobb Mountain area. Both of our samples from this unit yielded indistinguishable ages (1.16 ± 0.02 and 1.15 ± 0.02 Ma respectively; Table 1). The stratigraphically intermediate (CMD) and youngest (CVD) samples in turn yield weighted average $^{40}\text{Ar}/^{39}\text{Ar}$ ages of 1.10 ± 0.02 and 1.00 ± 0.05 Ma respectively. All of these ages agree within uncertainty (95% confidence level) with previously published K-Ar (Mankinen et al., 1978; Donnelly-Nolan et al., 1981) and $^{40}\text{Ar}/^{39}\text{Ar}$

(Turrin et al., 1994) ages determined for these rocks. Overall, the time span indicated for eruption from the Cobb Mountain edifice (0.15 ± 0.06 Ma) appears to have been somewhat more protracted than that previously indicated by K-Ar analysis (0.06 ± 0.04 Ma; Mankinen et al., 1978). In contrast, our $^{40}\text{Ar}/^{39}\text{Ar}$ age for the dacite of Tyler Valley (0.67 ± 0.01 Ma) is significantly younger than previously published K-Ar ages (0.86 ± 0.02 and 0.82 ± 0.02 Ma; Donnelly-Nolan et al., 1981), whereas our $^{40}\text{Ar}/^{39}\text{Ar}$ dating of sanidine constrains a somewhat older age for rhyolite of Pine Mountain (2.17 ± 0.02 Ma) than previously determined (2.06 ± 0.02 Ma) (Donnelly-Nolan et al., 1981). Potential pitfalls in Ar-dating such as incorporation of magma-derived ^{40}Ar in melt inclusions (e.g., Winick et al., 2001) or xenocrystic contamination do not appear to have adversely affected our results. For example, $^{40}\text{Ar}/^{36}\text{Ar}$ ratios determined for trapped Ar by isochron analysis overlap atmospheric composition within error and all calculated mean squared weighted deviates (MSWD) values are within or slightly

Table 3. Results of U-Pb zircon ion microprobe dating for Geysers-Cobb Mountain volcanic rocks

Sample ^a	Unit	Number			²⁰⁷ Pb/ ²⁰⁶ Pb ^b		²³⁸ U/ ²⁰⁶ Pb model age [Ma] ^b			²³⁸ U/ ²⁰⁶ Pb model age [Ma] ^c			²³⁸ U/ ²⁰⁶ Pb model age [Ma] ^d		²³⁸ U/ ²⁰⁶ Pb model age [Ma] ^e			
		spots	grains	excluded	$\pm 1 \sigma$	not disequilibrium corrected			disequilibrium corrected			$\pm 1 \sigma$	MSWD	$\pm 1 \sigma$	MSWD			
						$\pm 1 \sigma$	MSWD		$\pm 1 \sigma$	MSWD						$\pm 1 \sigma$	MSWD	
Pine Mountain PM0102A	Rhyolite of Pine Mountain	10	10	–	0.81	0.12	2.38	0.04	1.0	2.31	0.04	1.0	2.47	0.04	1.0	2.46	0.03	0.8
Cobb Mountain KA5431	Rhyolite of Alder Creek	27	20	–	0.86	0.06	1.30	0.06	9.9	1.24	0.12	10.1	1.40	0.06	9.9	1.36	0.02	5.9
CM0002	Rhyolite of Alder Creek	26	24	2 ^f	0.79	0.03	1.24	0.03	2.2	1.20	0.06	3.9	1.33	0.03	2.2	1.32	0.01	1.5
ACR2	Rhyolite of Alder Creek	21	21	1 ^f	0.88	0.05	1.30	0.03	3.9	1.10	0.11	5.9	1.39	0.03	3.9	1.36	0.02	1.9
all ACR	Rhyolite of Alder Creek	74	65	3 ^f	0.83	0.01	1.29	0.01	5.7	1.20	0.06	7.3	1.38	0.01	5.7	1.35	0.01	3.3
CM0004	Rhyodacite of Cobb Mountain	20	15	–	0.84	0.04	1.23	0.04	3.9	1.16	0.06	4.2	1.33	0.04	3.9	1.31	0.02	2.6
CM0003	Dacite of Cobb Valley	22	17	3 ^f	0.94	0.12	1.17	0.03	3.2*	1.16	0.06	3.0	1.27	0.03	3.2	1.26	0.02	2.1
Tyler Valley TV0101	Dacite of Tyler Valley	15	10	–	0.74	0.05	0.85	0.01	5.3*	0.80	0.08	3.8	0.94	0.03*	0.95	0.03	4.2	

^a location see Table 1; ACR2 longitude: 122.7628 latitude: 38.8002.

^b Y–intercept and concordia intercept age (*for regression $R^{7/6}_c$ fixed at 0.8283).

^c ²⁰⁴Pb–corrected age ($R^{4/6}_c = 18.8$).

^d modified concordia intercept age ($D_{Th/U}^{zircon/melt} = 0.17$).

^e ²⁰⁷Pb– and disequilibrium corrected age ($D_{Th/U}^{zircon/melt}$ from analysis; $Th/U_{melt} = 2.3$).

^f pre–Quaternary.

all errors analytical only scaled by the square–root of the MSWD.

below the expected range for the 95% confidence interval (e.g., Mahon, 1996).

4.3. Zircon U-Pb Ages

4.3.1. ^{204}Pb -corrected ages and xenocrysts

A summary of the U-Pb results for all units studied is presented in Table 3. Zircon U and Th contents are summarized in Figure 5. Results of individual analyses are available from http://oro.ess.ucla.edu/labdata/data_repository.html. When conventionally interpreted (i.e., using measured ^{204}Pb as a proxy for common lead; Compston et al., 1984), more than 97% of the 141 spot analysis results yielded poorly to well-resolved Pliocene-Pleistocene ages (Fig. 7). Three out of five weighted averages of the ^{204}Pb -corrected ages (Fig. 7) are reversely discordant or even yield $^{207}\text{Pb}/^{235}\text{U}$ ages <0 . This and the observed scatter of the ^{204}Pb -corrected results are primarily related to the difficulty in making the common Pb correction and not a consequence of U-Pb inheritance or initial disequilibrium.

In most instances, CL images revealed simple zoning patterns within euhedral zircons (Fig. 3a). Grains from CVD are typically rounded indicating partial resorption (Fig. 3b,c). Resolvable inherited cores and later overgrowths were identified in only a few instances (Fig. 3c,d). Overgrown cores and xenocrystic grains in the volcanic samples are in fact quite easily distinguished by their markedly older ages (between 90 to 150 Ma; see Fig. 4 in the companion paper Schmitt et al., this issue) that are similar to those from Jurassic to Late Cretaceous Franciscan wall rocks (Mattinson, 1988).

4.3.2. Alternative corrections for common Pb

Clearly, a different method to correct for common Pb is required to further refine the results displayed in Figure 7. We explored two approaches that both assume concordance of the U-Pb systematics. While such an assumption may be a poor one in many settings (e.g., Black et al., 1986), we feel that it is easily justified in the case of the Geysers - Cobb Mountain zircons because inherited grains and/or overgrown cores were so readily identifiable.

Getty and DePaolo (1995) have demonstrated that it is quite reasonable to use ^{207}Pb as a proxy for common Pb for Quaternary rocks because radiogenic $^{207}\text{Pb}/^{206}\text{Pb}$ ($R_c^{7/6}$) is almost invariant for Quaternary samples with only $\sim 0.1\%$ increase from the present-day production ratio of 0.0461. In the case of our ion microprobe measurements, common Pb was dominantly contributed from the surfaces of our samples (see 4.3.4). We consequently used an anthropogenic common $^{207}\text{Pb}/^{206}\text{Pb}$ ratio ($R_c^{7/6}$) of 0.8283 (Sañudo-Wilhelmy and Flegal, 1994). This ^{207}Pb -correction approach has the advantage that the disequilibrium-corrected $^{206}\text{Pb}^*/^{238}\text{U}$ (see 4.3.3.) can be calculated for each individual analysis.

A second approach pioneered by Baldwin and Ireland (1995) is to regress the data uncorrected for common Pb on a concordia plot. We used a $^{207}\text{Pb}/^{206}\text{Pb}$ vs. $^{238}\text{U}/^{206}\text{Pb}$ diagram that has the advantage that the errors between measured $^{207}\text{Pb}/^{206}\text{Pb}$ and $^{238}\text{U}/^{206}\text{Pb}$ are essentially uncorrelated. If the results reflect mixing between a single radiogenic U-Pb reservoir and a fixed common Pb contaminant, they are expected to produce a well-

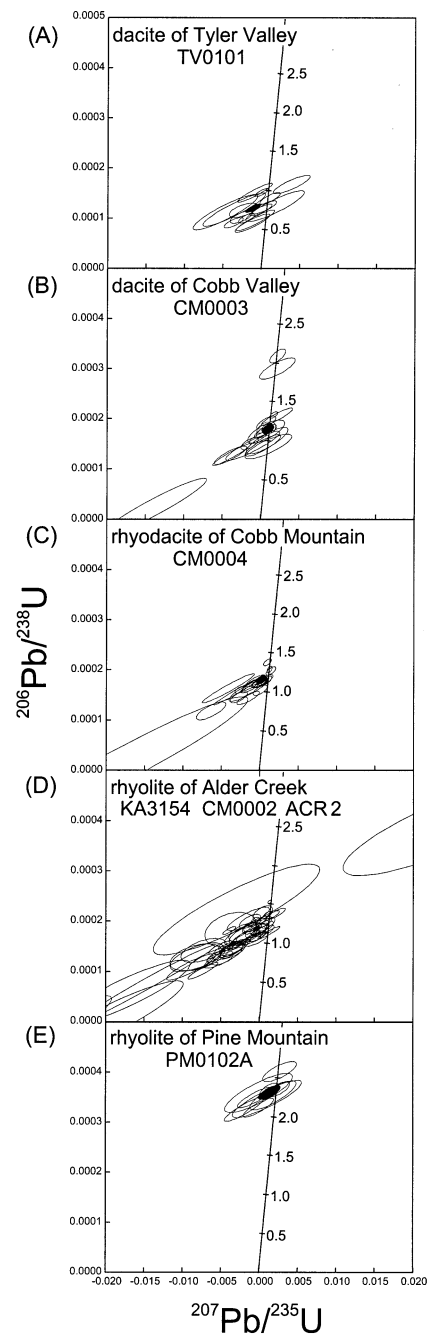


Fig. 7. $^{206}\text{Pb}/^{238}\text{U}$ vs. $^{207}\text{Pb}/^{235}\text{U}$ for The Geysers - Cobb Mountain volcanic zircons (^{204}Pb -corrected for common Pb). The individual analysis results are plotted as open (1σ errors) and weighted averages as filled ellipses (at 95% confidence interval). Equilibrium concordia line is drawn for age range between 0 and 3 Ma.

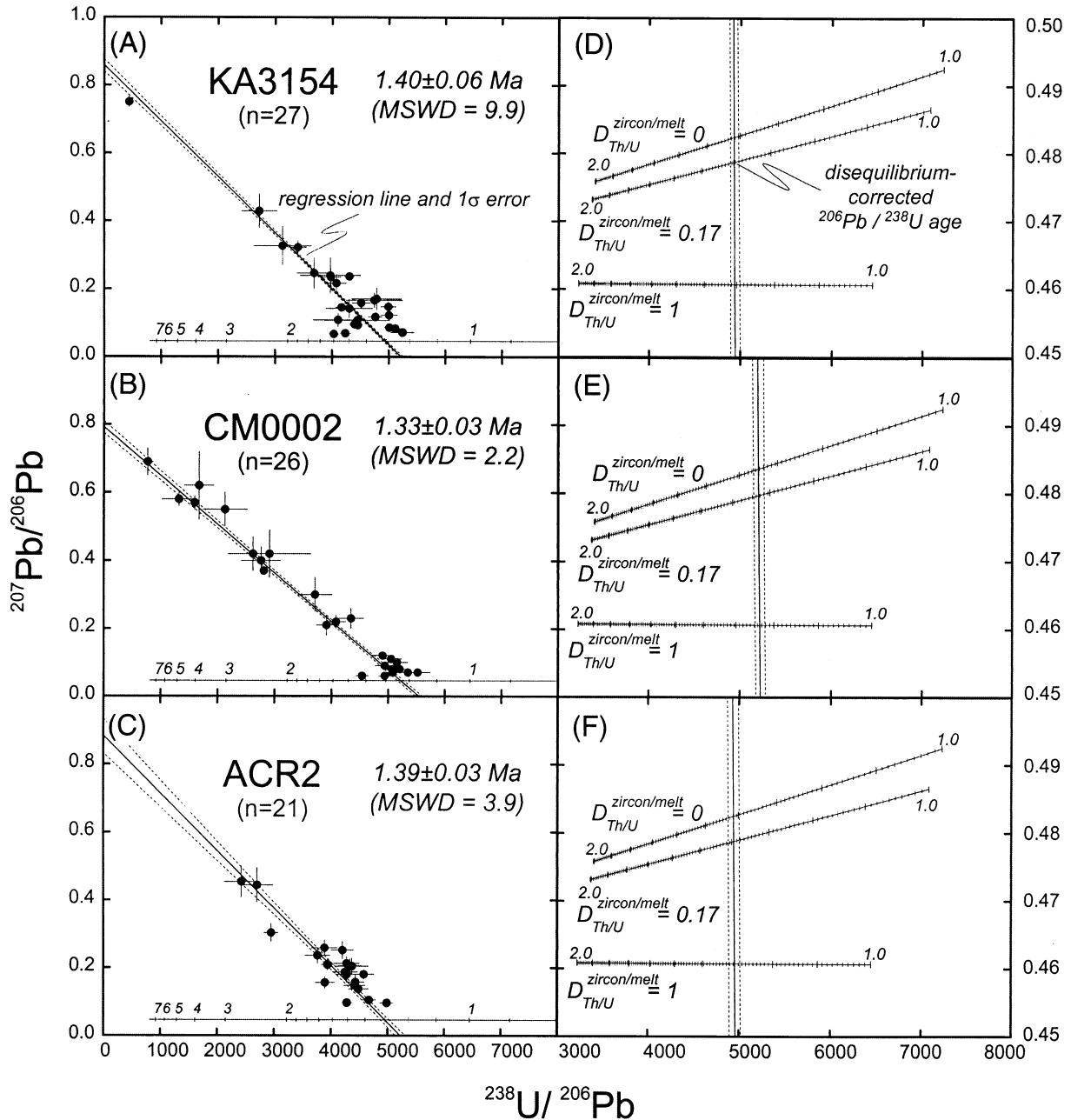


Fig. 8. $^{207}\text{Pb}/^{206}\text{Pb}$ vs. $^{238}\text{U}/^{206}\text{Pb}$ of ACR zircons (uncorrected for common Pb; error bars 1σ) showing regression line with 1σ error hyperbola (a–c). Note that pre-Quaternary grains ($n = 3$ of 65 total) have been excluded in the regression. Panels on right-hand side (d–e) illustrate effect of initial disequilibrium on the concordia intercept ages for the same regression. Intercept ages vary as a function of the fractionation of Th and U in zircon crystallizing from a melt. For example, complete disequilibrium (i.e., no initial ^{230}Th) would cause intercept ages to increase by roughly 0.1 Ma or 10% relative (upper curve) compared to equilibrium conditions (lower curve). Reported model ages in Table 3 were calculated using a zircon mineral-melt distribution coefficient ($D_{\text{zircon/melt}}^{\text{Th/U}}$) of 0.17, estimated from Th/U in whole-rocks, melt inclusions and zircon (middle curve).

defined, linear array whose y-axis intercept corresponds to the common $^{207}\text{Pb}/^{206}\text{Pb}$ ratio and whose intercept with concordia yields the U-Pb age.

Concordia intercept ages and common $^{207}\text{Pb}/^{206}\text{Pb}$ ratios determined for three samples from the ACR (two of which

yielded coeval $^{40}\text{Ar}/^{39}\text{Ar}$ ages; see previous section) overlap within error (Fig. 8 and Table 3). We note, however, that MSWD values are relatively high and may potentially indicate more than one component or an extended crystallization interval in the Quaternary zircon population (see 4.3.4.).

Finally, to check for potential instrumental bias, we also analyzed CM0002 and KA3154 zircon grains ($n = 16$) on a separate mount using the SHRIMP RG ion microprobe at the Australian National University. Ages overlapping in error were obtained after applying the alternative correction methods described above (intercept age uncorrected for disequilibrium: 1.26 ± 0.03 Ma, MSWD = 0.5; cf., Table 3).

4.3.3. Correction for the effects of initial U-Pb disequilibrium

Although $^{207}\text{Pb}/^{206}\text{Pb}$ vs. $^{238}\text{U}/^{206}\text{Pb}$ arrays produced by young zircons intersect concordia at a steep angle, it is difficult to precisely know the position of concordia in Figure 7 and Figure 8 because its coordinates depend upon the initial excesses or deficits of intermediate daughter products in the U-Pb decay chains (Mattinson, 1973; Ludwig, 1977; Schärer, 1984; Wendt and Carl, 1985). It is possible to exploit the disturbance of the U-decay system caused by Th/U fractionation to perform disequilibrium dating of zircon in <300 ka volcanic rocks (e.g., Fukuoka and Kigoshi, 1974; Reid et al., 1997; Charlier and Zellmer, 2001). Similarly, some Quaternary zircons analyzed by U-Pb methods yielded apparent ages that postdate eruption ages when uncorrected for isotopic disequilibrium (e.g., Brown and Fletcher, 1999; Reid and Coath, 2000).

In the case of zircon, initial disequilibrium between parent and intermediate daughters in the U-decay chain can be produced by mineral-melt fractionation between the long-lived U-isotopes (^{238}U and ^{234}U) and ^{230}Th ($t_{1/2} \sim 75$ ka) during zircon crystallization. With appropriate data (i.e., measured Th and U abundances in zircon, melt inclusion glasses and whole-rocks), it is possible to estimate the degree of fractionation of Th from U and the resulting effect upon U-Pb age following the method outlined in Schärer (1984). The effects of ^{230}Th disequilibrium outweigh potential deficits in other short-lived intermediate daughter products such as ^{226}Ra during the crystallization of zircon and can be reasonably neglected. Disequilibrium in the ^{235}U decay chain could be caused by the longest-lived daughter ^{231}Pa ($t_{1/2} \sim 30$ ka). The resulting effects, however, are also of minor importance, because limited ingrowth of ^{207}Pb due to the present-day scarcity of ^{235}U relative to ^{238}U causes concordia to assume a trajectory that is essentially parallel to the $^{238}\text{U}/^{206}\text{Pb}$ axis for the Late Cenozoic. As a consequence, shifts in the position of concordia produced by initial disequilibrium in the $^{207}\text{Pb}/^{235}\text{U}$ decay chain are in a direction that is nearly parallel to U-Pb arrays defined by young zircon samples and therefore will have negligible impact upon the intercept age.

All ^{207}Pb -corrected $^{206}\text{Pb}^*/^{238}\text{U}$ ratios in this study have been individually adjusted for initial disequilibrium by multiplying $^{206}\text{Pb}^*$ with $(1 + \phi)$, where the factor ϕ is defined by $(^{206}\text{Pb}/^{238}\text{U})_{\text{disequilibrium}} / (^{206}\text{Pb}/^{238}\text{U})_{\text{equilibrium}}$. Since we only consider ^{230}Th deficiency as relevant for zircon, we estimated $(^{206}\text{Pb}/^{238}\text{U})_{\text{disequilibrium}}$ from $(1 - D_{\text{Th/U}}^{\text{zircon/melt}}) \times 1.7 \cdot 10^{-5}$ ($1.7 \cdot 10^{-5} = ^{230}\text{Th}/^{238}\text{U}$ at secular equilibrium) whereas $(^{206}\text{Pb}/^{238}\text{U})_{\text{equilibrium}}$ equals the equilibrium daughter/parent ratio at the age derived from $^{206}\text{Pb}^*/^{238}\text{U}$ ($D_{\text{Th/U}}^{\text{zircon/melt}}$ = ratio of zircon mineral-melt partition coefficients for Th and U). From the data shown in Figure 5 we determined an average value of 0.17 ± 0.08 for $D_{\text{Th/U}}^{\text{zircon/melt}}$. Note that while glass inclusion

and whole rock values of Th/U are relatively constant (weighted average 2.3 ± 0.1), more variable ratios between 0.15 and 1.2 were obtained from zircon (Fig. 5).

Our average value for $D_{\text{Th/U}}^{\text{zircon/melt}}$ is about five times higher than the value we calculated for 800°C by solving the algorithm of Blundy and Wood (1994) for U^{4+} and Th^{4+} in octahedral coordination using bulk modulus data from Hazen and Finger (1979). Compared to the ~ 6 – 8% increase in age caused by initial deficit in ^{230}Th , the discrepancy between predicted and observed $D_{\text{Th/U}}^{\text{zircon/melt}}$ has only relatively minor impact on the resulting age correction ($+0.09$ or $+0.11$ Ma, respectively, for a 1.3 Ma zircon). Similarly, uncertainties arising from potential complications such as $(^{230}\text{Th})/(^{238}\text{U})_{\text{melt}}/1$ (melt disequilibrium) can only be estimated from comparison with measured values of $(^{230}\text{Th})/(^{238}\text{U})_{\text{melt}}$ preferably from Holocene rhyolites (cf., Reid et al., 1997), because the rocks investigated in this study are too old to experimentally test the assumption of melt equilibrium. Because $(^{230}\text{Th})/(^{238}\text{U})_{\text{melt}}$ is typically >1 , these effects would systematically decrease the disequilibrium corrected ages by $<1\%$ in reasonable limits for $(^{230}\text{Th})/(^{238}\text{U})_{\text{melt}}$ inferred from Reid et al. (1997). Compared to our estimate of the external variability observed for zircons from three separate ACR samples ($\sim 3\%$; see 4.3.5.), these additional sources of uncertainty are negligible.

4.3.4. U-Pb results from standard zircon 61.308A

To check the precision and accuracy of our ion microprobe approach for Late Cenozoic zircons, we have examined a reference zircon (61.308A; Wiedenbeck et al., 1995). This material yielded a $^{206}\text{Pb}/^{238}\text{U}$ weighted average age of 2.488 ± 0.004 (MSWD = 4.3) at reported U contents of 158 ppm analyzed by conventional isotope dilution and thermal ionization mass spectrometry (Wiedenbeck et al., 1995). We obtained a concordia intercept age of 2.58 ± 0.05 Ma (MSWD = 1.2) and $R_c^{7/6} = 0.91 \pm 0.08$ from a regression through the data uncorrected for common Pb (Fig. 9). By systematically increasing the primary beam intensity and progressively blocking ions generated around the periphery of the pit by reducing an aperture diameter in the secondary ion path (field aperture), we reduced $^{207}\text{Pb}/^{206}\text{Pb}$ from ~ 0.4 to values that overlap with concordia within error. This observation and the comparatively strong decay of the ^{204}Pb and ^{207}Pb intensities during the first few minutes of the analysis supports our contention that the $R_c^{7/6}$ values we have determined are not geologically meaningful but simply a consequence of surface lead contributed from the periphery of the ion craters which was most likely introduced during sample preparation and polishing.

Because the spread along the y-axis was comparatively limited, we also employed a regression using a fixed y-axis intercept with $R_c^{7/6} = 0.8283$ (anthropogenic Pb for Los Angeles Basin; Sañudo-Wilhelmy and Flegal, 1994). This yielded a slightly younger concordia intercept age of 2.54 ± 0.06 Ma (MSWD = 1.2). Both, the intercept and the ^{207}Pb -corrected weighted average age for 61.308A (2.52 ± 0.04 Ma; MSWD = 1.0) are indistinguishable from the conventionally determined $^{206}\text{Pb}/^{238}\text{U}$ age within measurement uncertainties. In contrast, a lower and comparatively imprecise $^{206}\text{Pb}/^{238}\text{U}$ age is obtained if ^{204}Pb is used as a proxy for common Pb (2.33 ± 0.09 Ma;

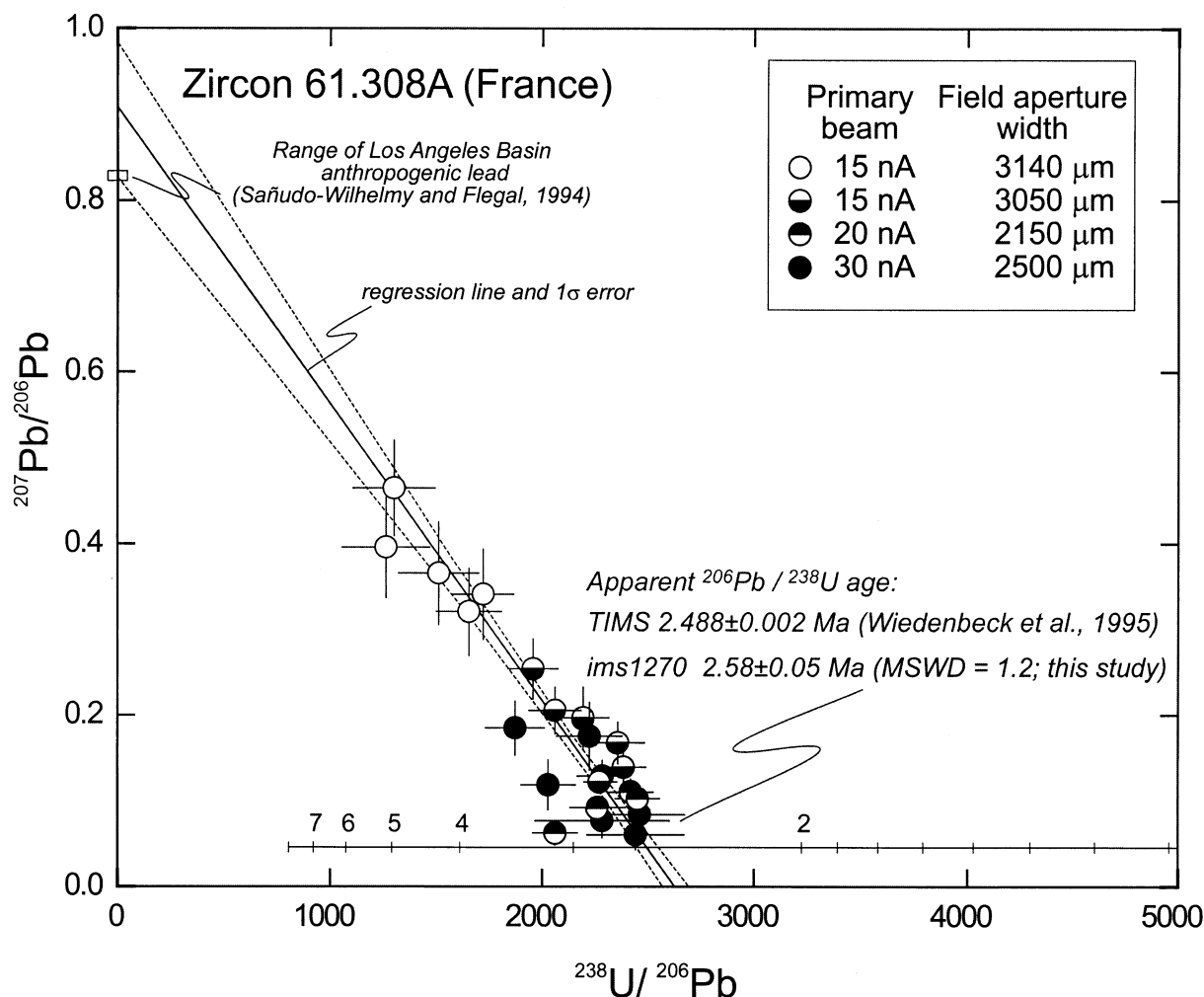


Fig. 9. $^{207}\text{Pb}/^{206}\text{Pb}$ vs. $^{238}\text{U}/^{206}\text{Pb}$ from reference zircon 61.308A (France) uncorrected for common Pb (1σ error bars). Symbols refer to instrumental conditions (primary beam current and field aperture width) that were varied to optimize transmission and that resulted in variable contributions of surficial Pb from sputter-crater edges. Regression through the uncorrected data yields common $^{207}\text{Pb}/^{206}\text{Pb}$ ratio (y-intercept) and an apparent age from the intercept with Concordia (quoted with 1σ errors). Note overlap of common $^{207}\text{Pb}/^{206}\text{Pb}$ with anthropogenic values (Sañudo-Wilhelmy and Flegal, 1994).

MSWD = 1.9). Based upon our results from 61.308A we conclude that the accuracy of both the concordia intercept and ^{207}Pb -corrected weighted averages of $^{206}\text{Pb}/^{238}\text{U}$ ages derived from Geysers – Cobb Mountain zircons should be comparable to the typical $\pm 3\%$ or less (1σ) reproducibility we observed in the standard analyses used for calibration.

4.3.5. Geysers - Cobb Mountain area

Zircon U-Pb model ages calculated for samples from the Cobb Mountain area are provided in Table 3 (weighted averages of concordia intercept and ^{204}Pb -corrected U-Pb ages; uncertainties stated as $\pm 1\sigma$ standard errors calculated from analytical errors and MSWD values). The compilation also includes the disequilibrium-corrected U-Pb ages (concordia intercept and ^{207}Pb -corrected) calculated as described above. Regardless of the calculation approach employed, both disequilibrium-corrected U-Pb zircon model ages in Table 3 agree

quite closely and decrease in a manner that is consistent with the sequence of eruption ages inferred from stratigraphy and $^{40}\text{Ar}/^{39}\text{Ar}$ dating (Table 1). Note that in calculating these model ages, we omitted four Jurassic-Cretaceous grains and two analyses in which the ion probe crater overlapped with Cretaceous cores.

Results from each of the five volcanic samples are sufficiently well-defined to compare their zircon age populations (Figs. 10 and 11). It is clear that the zircon U-Pb age populations of the Cobb Mountain suite (ACR, CMD, and CVD in Fig. 11b–d) are dissimilar to those yielded by the rhyolite of Pine Mountain (Fig. 11e) and dacite of Tyler Valley (Fig. 11a). Within the Cobb Mountain suite zircon U-Pb age distributions overlap significantly (Fig. 10 and Fig. 11b–d) and show strong similarity to those determined from the main intrusive phase of the GPC (Fig. 11f; see also Schmitt et al., this issue). Interestingly, none of the volcanic units exhibit any evidence for zircon

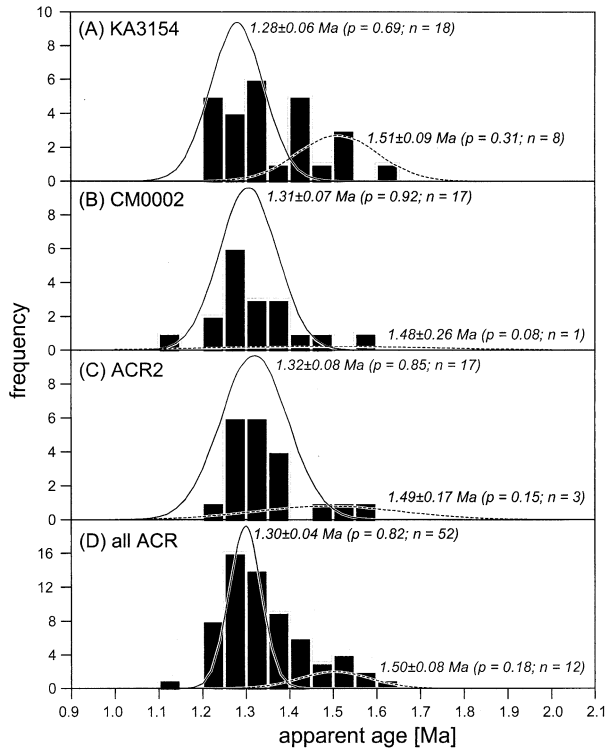


Fig. 10. Histograms of ^{207}Pb -common-Pb and disequilibrium corrected zircon ages of three individual samples from the rhyolite of Alder Creek (a–c). Pooled data from these samples are presented in bottom panel (d). Normalized gaussian probability curves were calculated from the results of two-component mixture modeling (Sambridge and Compston, 1994) and illustrate the two maximum likelihood ages (maximum of curve) and their relative proportions p (areas under the curves).

carry-over from the earliest ~ 1.8 Ma magmatic phase of the GPC (microgranite porphyry in Fig. 11g).

Each of the model ages presented in Table 3 assumes that zircons from a given sample represent a single age population. Hence it is problematic that in nearly all cases, the associated MSWD values exceed maximum allowable limits (at the 95% confidence level) for a single age population (e.g., Mahon, 1996). Because, unrecognized analytical factors could be responsible for the elevated MSWD values in Table 3, a conservative way of dealing with the elevated MSWD values involves scaling the errors in Table 3 by the square root of the MSWD to ensure that they adequately represent the excess scatter. While we have elected to take this approach, it is also quite possible that we are obscuring a meaningful geologic signal by describing our results in terms of single age populations.

To better evaluate the possibility that multiple age populations are manifested in our results, we have more closely examined data obtained from the three ACR samples. These exhibit the most elevated MSWD values and collectively account for a substantial fraction of the U-Pb data we gathered in this study. Histograms calculated for each of the three samples reveal non-unimodal age distributions (Fig. 10a–c). When we pooled all results from ACR and applied the algorithm of Sambridge and Compston (1994), we determined a best-fit two-component model with a dominant ($\sim 80\%$) peak at $1.30 \pm$

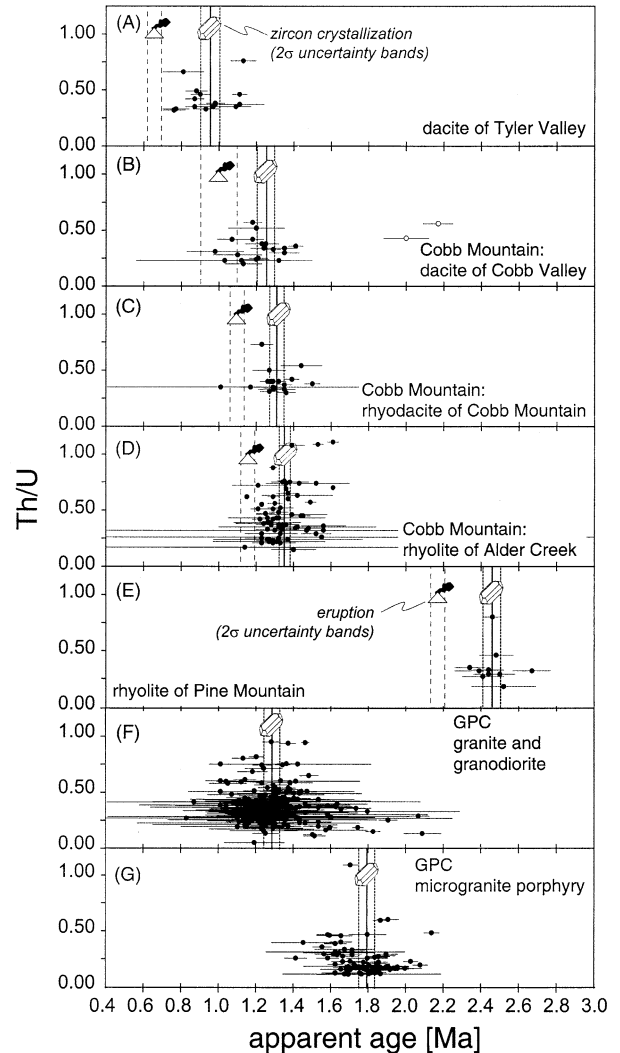


Fig. 11. Summary of Th/U vs. ^{207}Pb -common Pb and disequilibrium corrected crystallization ages for volcanic (a–e) and plutonic (f and g) samples from the Geysers – Cobb Mountain system (Schmitt et al., this issue). Eruption ages from $^{40}\text{Ar}/^{39}\text{Ar}$ sanidine dating are shown for comparison and indicate preeruptive zircon storage for ~ 0.2 – 0.3 Ma (error bars for individual analyses at 1σ level).

0.04 Ma and a minor ($\sim 20\%$) peak at 1.50 ± 0.08 Ma (Fig. 10d). However, note that these two age components are resolved only at the 85% confidence level in the composite sample ($n = 64$) and by lesser margins in the individual samples (Fig. 10a–c). In light of this, we think that there is insufficient evidence to conclude that two distinct age populations are necessarily exhibited by these samples.

5. DISCUSSION

5.1. Significance of Zircon Residence Times

Determining the petrogenetic significance of U-Pb zircon ages from volcanic rocks can be a difficult task. While potassium-argon ages of volcanic sanidine are conventionally expected to date the time of eruption (McDougall and Harrison,

1999), diffusion of U, Th, and Pb in zircon is sufficiently slow for closure at magmatic temperatures, so that crystallization ages may be recorded (Watson et al., 1997; Cherniak and Watson, 2001). Several recent ion microprobe study of zircons from Quaternary rhyolites (e.g., Long Valley: Reid et al., 1997; Reid and Coath, 2000; Taupo: Brown and Fletcher, 1999; Yellowstone: Bindeman et al., 2001; Vazquez and Reid, 2002) have reported a resolvable time interval (≥ 0.06 Ma) between zircon crystallization and the eruption age based on the results from zircon U-Pb and sanidine $^{40}\text{Ar}/^{39}\text{Ar}$ geochronology.

The intervals we have determined between crystallization (zircon U-Pb age) and eruption (sanidine $^{40}\text{Ar}/^{39}\text{Ar}$ ages) for the Pine Mountain (0.30 ± 0.07 Ma), ACR (0.23 ± 0.02 Ma), CMD, (0.23 ± 0.06 Ma), CVD (0.27 ± 0.08 Ma), and Tyler Valley (0.27 ± 20 Ma) units are in line with results determined in the above-mentioned studies (stated errors are total $\pm 1\sigma$ uncertainties). This conclusion holds even if multiple zircon U-Pb age populations are present (as is potentially the case for ACR, see Fig. 10) and we emphasize that the existence of an older age population is not inconsistent with our conclusions since we have recognized intrusions with ~ 1.45 Ma zircons within the GPC (see Schmitt et al., this issue). Our observation that relatively large intervals of pre-eruptive zircon residence ($\sim 0.2 - 0.3$ Ma) are associated with small volume eruptive units ($< 10 \text{ km}^3$; Hearn et al., 1995) agrees with the findings of the previous studies. For example, Reid et al. (1997) documented more protracted zircon residence (> 0.1 Ma) for small-volume rhyolites than did Reid and Coath (2000), Bindeman et al. (2001), and Vazquez and Reid (2002) for much larger volume ($> 100 \text{ km}^3$) ignimbrites. It should be emphasized that the volcanics we have studied are underlain by the $> 300 \text{ km}^3$ GPC which is comparable in volume to many caldera-forming rhyolites.

While the interpretation that the interval between zircon U-Pb ages and $^{40}\text{Ar}/^{39}\text{Ar}$ eruption ages record crystal residence times in a shallow magma chamber has been widely accepted (e.g., Reid et al., 1997; Brown and Fletcher 1999; Bindeman et al., 2001; Vazquez and Reid, 2002), alternative explanations for this phenomenon exist. For example, crystals in silicic magmas may form during different stages of magma production, ascent, or storage at different crustal levels (cf. Smith, 1979; Hildreth, 1981; Huppert and Sparks, 1988). If zircons crystallize in a deep-seated melt generation zone, the interval between zircon U-Pb ages and $^{40}\text{Ar}/^{39}\text{Ar}$ eruption ages will overestimate their residence in the shallow magma chamber. Moreover, zircons may not even record magma residence at all. Specifically, zircon crystals can be salvaged from just-solidified plutonic roots of magma systems by remelting in response to magmatic re-injection (e.g., Lowenstern et al., 2000; Bindeman et al., 2001).

In the light of the controversy regarding the heat-source for the long-lived Geysers geothermal system, it is particularly important to better understand the significance of zircon residence times in the Geysers – Cobb Mountain system. Isherwood (1981) and McLaughlin (1981) envisioned a long-lived, continuously molten magma chamber (represented in part by the GPC). Alternatively, others (McLaughlin et al., 1983; Williams et al., 1993; Kennedy and Truesdell, 1996; Stanley et al., 1998; Stimac et al., 2001) have all argued for episodic intrusion of smaller bodies throughout the Geysers region to explain the

elevated heat flow and hydrothermal activity. Although our geochronologic data are broadly consistent with either scenario, we will argue on the basis of geochemical and thermochronologic data for the GPC that continuous residence of zircons in a magma from the time they crystallized to the eruption is unlikely for the Cobb Mountain volcanic center.

5.2. Where Did Zircons Crystallize?

In our analysis of the conditions for zircon growth, we will focus upon the ACR magma since it is the volumetrically most significant unit of the Cobb Mountain center and because it is compositionally equivalent to the dominant plutonic unit of the GPC (orthopyroxene-biotite granite; Schmitt et al., this issue). Our results imply that the melt was undersaturated with respect to zircon at the time inclusions were trapped in quartz (Fig. 6). Specifically, the low and variable zircon saturation temperatures we determined for the quartz-hosted melt inclusions (relative to whole-rock values) are inconsistent with zircon - melt equilibrium at magmatic temperatures, because the presence of zircon would buffer Zr abundance in the melt.

Correlation between Zr and Nb (Fig. 6) further rules out the possibility that quartz trapped an initially zircon-saturated melt at low temperatures ($< 750^\circ \text{C}$) that later became undersaturated as a result of a temperature increase before eruption. This correlation also precludes experimental artifacts such as incomplete dissolution of zircon during laboratory rehomogenization, since Nb is expected to behave incompatibly even in the presence of zircon. Enrichment due to the incompatible behavior of Nb and Zr in crystallizing major phases (mainly feldspar, quartz, and biotite) could have produced the observed trends, but the overall enrichment in Zr (1.2-fold) and Nb (4.5-fold) would either require extreme fractionation ($0.03 < f < 0.10$; f = mass of melt remaining/original mass of melt) or could have resulted from rapid melt extraction from the source region that did not allow for equilibration between melt and residual accessory phases in the restite. Either way, it appears that at the time of inclusion entrapment the ACR melt was very low in Zr and thus zircon undersaturated at magmatic temperatures of $\sim 780^\circ \text{C}$ as indicated by our two feldspar thermometry.

We estimate that the amount of crystallization needed to saturate such a low-Zr melt in zircon is for $f < 0.75$ on the basis of the highest Zr contents we have measured from the melt inclusions (89 ppm). This assumes Zr incompatibility in all other phases and a magmatic temperature of $\sim 780^\circ \text{C}$. Note that considerably higher degrees of crystallization ($f < 0.5$) are required to saturate a melt with initially only ~ 50 ppm (or less) Zr as indicated by the majority of the melt inclusions (Fig. 6). Our interpretation that the melt was zircon undersaturated before crystallization is further supported by the scarcity of pre-Quaternary zircons. Of the 117 zircons analyzed in this study, only four pre-Quaternary ages were measured and two of these exhibit textures that indicate initial resorption and later overgrowth (Fig. 3c–d).

If our interpretation of the melt being zircon undersaturated at the time of inclusion entrapment is valid, it follows, on the basis of a variety of indirect considerations, that zircon crystallization most probable occurred at shallow levels. First, magma viscosities are known to increase sharply after crystal volumes exceed $\sim 25 - 40\%$ (Ryerson et al., 1988; Lejeune and

Richet, 1995). Thus extensive crystallization dramatically impedes ascent of crystal-rich magmas and it is easiest to imagine that the magma had reached shallow levels before most crystallization occurred. Second, variations in B and Cl abundance of melt inclusions suggest volatile-saturated conditions at the time of inclusion entrapment (Fig. 4). Again, we view it most likely that melt entrapment occurred at low pressures where volatile-saturated conditions are favored. Finally, compositionally equivalent plutonic rocks of the GPC were intruded as shallow as 1–2 km (Moore et al., 2000). As zircon saturation temperatures for these compositions fall below the solidus for water-saturated haplogranite (Johannes and Holtz, 1996; assuming lithostatic pressures between 27 and 53 MPa and using non-reservoir metagreywacke densities of 2700 kg/m³ from Gunderson, 1991) this would imply freezing of the melt before zircon crystallization. In our view, it thus seems far more likely that zircon crystallization took place in shallowly emplaced magma that was originally crystal-poor and zircon undersaturated rather than in a deep-seated magma generation zone.

5.3. Comparison with Cogenetic(?) Plutonic Zircons: Evidence for Remelting?

Disequilibrium-corrected U-Pb zircon results from Pine Mountain and Tyler Valley clearly indicate that these centers, although in close proximity to the Geysers field, were physically isolated from Cobb Mountain and the GPC. In contrast, the age range (~1.2–1.4 Ma) we determined for the rhyolitic to (rhyo-)dacitic volcanics erupted from Cobb Mountain closely overlaps with U-Pb ages obtained from the majority (95% by volume) of GPC plutonic samples (orthopyroxene-biotite granite and hornblende-pyroxene-biotite granodiorite in Fig. 10f; see also Schmitt et al., this issue). Interestingly, ~1.8 Ma zircons that characterize the shallow cap of the GPC (microgranite porphyry; Fig. 11g) are prominently absent. If the GPC intrusives and Cobb Mountain eruptives were sequentially tapped from a larger continuously differentiating magma body that reached zircon saturation ~1.8 Ma ago, we would expect zircons of this age in the younger magmas (cf. Reid et al., 1997). It therefore appears that zircons from the Cobb Mountain volcanics were largely derived from the main-phase GPC (see also Schriener and Suemnicht, 1981; Hulen and Nielson, 1993).

The difference between disequilibrium-corrected zircon U-Pb model ages and corresponding ⁴⁰Ar/³⁹Ar model ages for the volcanic rocks indicates that the temperature of the erupted magmas had decreased sufficiently to permit zircon crystallization about 0.2 Ma before eruption. Because temperature estimates for the onset of zircon crystallization (775–790° C; see Fig. 6) overlap with results from two-feldspar thermometry (750–820° C), either isothermal magma storage or cooling and remelting occurred during this ~0.2 Ma interval. K-feldspar thermochronology of GPC samples recovered from depths as great as 3–4 km indicate that the GPC had cooled well below solidus temperatures by about 1.2–1.0 Ma (Dalrymple et al., 1999), the interval over which the Cobb Mountain units were erupted. Moreover, plutonic rocks in the GPC preserve sharp compositional gradients and contrasting U-Pb zircon age populations across lithologic boundaries (see Schmitt et al., this issue). This indicates that individual magma batches crystal-

lized rapidly after emplacement and that no large convecting magma system persisted at the level of the GPC for intervals resolvable by our U-Pb dating technique. Similarly, numerical simulations of heat flow in the Geysers geothermal system indicate that a silicic magma chamber with a volume of ~300 km³ could not have been maintained above solidus conditions for more than 0.15 Ma at depths as shallow as 4 km, unless episodic recharge occurred (Norton and Hulen, 2001).

Thus, if the GPC was in fact the source of the Cobb Mountain eruptives, remelting of earlier intrusive rocks is indeed required by the observed plutonic thermal history (Hulen et al., 1997; Dalrymple et al., 1999) and by constraints from numerical heat-flow models (Norton and Hulen, 2001). As a geologically plausible explanation for this, we favor episodic recharge by mafic magma that supplied heat in the Geysers – Clear Mountain area (Stimac et al., 2001). Petrographic evidence for ubiquitous disequilibrium mineral paragenesis resulting from mixing between felsic and mafic magmas is widespread in Clear Lake volcanic rocks (A. Stimac, personal communication). Furthermore, isotopic disequilibrium of feldspar suggests mixing of crustal magmas with periodically injected mafic recharge (Futa et al., 1981). Reheating and mixing might also have caused partial resorption of preexisting young zircons in the CVD (see Fig. 3b,c). Our remelting interpretation is in line with the relatively small magma volumes erupted from the Geysers – Cobb Mountain system, their discontinuous compositional trends (i.e., early erupted rhyolites followed by intermediate compositions), and the intermittent eruption of basalt (i.e., the ~1.7 Ma Caldwell Pines) during the intrusion interval of the GPC (~1.8–1.1 Ma; Schmitt et al., this issue).

6. SUMMARY AND CONCLUSIONS

- (1) In this study, we presented a comprehensive data set of radiogenic isotopic measurements (K-Ar, U-Pb) supported by major and trace element data from a suite of volcanic rocks spatially associated with the hypabyssal GPC and the Geysers steam field. ⁴⁰Ar/³⁹Ar dating of sanidine constrains eruptive events that tapped (rhyo-)dacitic to rhyolitic magma between 2.17 ± 0.02 Ma (Pine Mountain), 1.15 ± 0.01 Ma to 1.00 ± 0.05 Ma (Cobb Mountain units) and 0.67 ± 0.01 Ma (Tyler Valley).
- (2) U-Th-Pb isotopic measurements of zircon were performed for the same samples. We used ratios of Th and U zircon-melt distribution coefficients ($D_{Th/U}^{zircon/melt} = 0.17 \pm 0.08$) determined from measured abundances in whole-rocks, quartz-hosted melt inclusions, and zircon to correct our ²⁰⁶Pb/²³⁸U zircon ages for initial ²³⁰Th disequilibrium. The resulting model ages significantly predate (by ~0.2–0.3 Ma) the eruption ages.
- (3) U-Pb zircon results from Pine Mountain and Tyler Valley demonstrate that these centers erupted materials that evolved physically isolated from the GPC and Cobb Mountain magma system. In contrast, the age range (~1.2–1.4 Ma) we determined for the rhyolitic to (rhyo-)dacitic volcanics erupted from Cobb Mountain closely overlaps with U-Pb ages obtained from the main-phase intrusions within the GPC. Older (~1.8 Ma) zircons characteristic of the upper levels of the GPC are absent in both the Cobb Mountain volcanics and the main-phase GPC. This sug-

gests that episodically emplaced intrusions rather than a single, large, long-lived, convecting magma chamber characterized the Geysers-Cobb Mountain magma system.

- (4) In the case of the rhyolite of Alder Creek, we find that Zr abundances in quartz-hosted melt inclusions are comparatively low and highly variable. This indicates that the melt was zircon undersaturated at the time of inclusion entrapment and that considerable crystallization (>25–50%) must have occurred before the melt reached saturation in zircon. Such a condition agrees with additional evidence indicating that the underlying GPC was emplaced at temperatures above zircon saturation.
- (5) Our model for the Geysers – Cobb Mountain magma system is as follows: Crystallization and zircon formation postdated ascent from the source region and occurred in upper-crustal magma reservoirs. The GPC was formed by aggregation of several relatively rapidly solidified magma batches. Episodic recharge of mafic magma thermally rejuvenated parts of the system, caused remelting of the GPC. Portions of the resulting partially hybridized magmas erupted from the Cobb Mountain volcanic center. This model is supported by a variety of further observations such as small eruptive volumes, discontinuous compositional variations, coeval basalt eruptions, and isotopic and textural evidence for magma mixing in the Cobb Mountain volcanic rocks.

Acknowledgments—This research was conducted under the auspices of Department of Energy grant DE-FG-03-89ER14049 and the instrumentation and facilities grant NSF grant EAR-0113563 to Harrison, McKeegan, and Reid. We thank Tom Box and Mitch Stark at Calpine for discussions and their support in securing samples from the Cobb Mountain area. Eric Cowgill ($^{40}\text{Ar}/^{39}\text{Ar}$) and Chris Coath (U-Pb) were instrumental in obtaining the isotopic age results. Ainslie Harrison aided in mineral separation. We thank Rudi Naumann (XRF), Oona Appelt (electron microprobe), Knut Hahne and Heike Rothe (ICP-MS) and Jörg Erzinger of the GeoForschungsZentrum Potsdam for their generous support. Critical comments on an earlier version of this manuscript by Julie Donnelly-Nolan, Bob McLaughlin and Jorge Vazquez are gratefully acknowledged. Comments by journal reviewers and editorial handling by Yuri Amelin helped to clarify this presentation.

Associate editor: Y. Amelin

REFERENCES

- Baker D. R., Conte A. M., Freda C., and Ottolini L. (2002) The effects of halogens on Zr diffusion and zircon dissolution in hydrous metaluminous granitic melts. *Contrib. Mineral. Petrol.* **142**, 666–678.
- Baldwin S. L. and Ireland T. R. (1995) A tale of two eras: Pliocene-Pleistocene unroofing of Cenozoic and late Archean zircons from active metamorphic core complexes, Solomon Sea, Papua New Guinea. *Geology* **23**, 1023–1026.
- Benz H. M., Zandt G., and Oppenheimer D. H. (1992) Lithospheric structure of northern California from teleseismic images of the upper mantle. *J. Geophys. Res.* **94**, 4791–4807.
- Bindeman I. N., Valley J. M., Wooden J. L., and Persing H. M. (2001) Post-caldera volcanism: In situ measurement of U-Pb age and oxygen isotope ratio in Pleistocene zircons from Yellowstone caldera. *Earth Planet. Sci. Lett.* **189**, 197–206.
- Black L. P., Williams I. S., and Compston W. (1986) Four zircon ages from one rock: The history of a 3930 Ma-old granulite from Mount Sones, Enderby Land, Antarctica. *Contrib. Mineral. Petrol.* **94**, 427–437.
- Blackwell D. D. and Steele J. L. (1992) *DNAG Geothermal Map of North America*. (1:5,000,000). Geol. Soc. Am., Boulder, Colorado.
- Blundy J. and Wood B. (1994) Prediction of crystal-melt partition coefficients from elastic moduli. *Nature* **372**, 452–454.
- Borg L. E. and Clyne M. A. (1998) The petrogenesis of felsic calc-alkaline magmas from the southernmost Cascades, California: Origin by partial melting of basaltic lower crust. *J. Petrol.* **39**, 1197–1222.
- Brown S. J. A. and Fletcher I. R. (1999) SHRIMP U-Pb dating of pre-eruption growth history of zircons from the 340 ka Whakamaru Ignimbrite, New Zealand: Evidence for >250 k. y. magma residence times. *Geology* **27**, 1035–1038.
- Cebula G. T., Kunk M. J., Mehnert H. H., Naeser C. W., Obradovich J. D., and Sutter J. F. (1986) The Fish Canyon Tuff, a potential standard for the $^{40}\text{Ar}/^{39}\text{Ar}$ and fission-track dating methods. *Terra Cognita* **6**, 139–140.
- Charlier B. and Zellmer G. (2001) Some remarks on U-Th mineral ages from igneous rocks with prolonged crystallisation histories. *Earth Planet. Sci. Lett.* **183**, 457–469.
- Cherniak D. J. and Watson E. B. (2001) Pb diffusion in zircon. *Chem. Geol.* **172**, 5–24.
- Compston W., Williams I. S., and Meyer C. (1984) U-Pb geochronology of zircons from lunar breccia 73217 using a sensitive high mass-resolution ion microprobe. *J. Geophys. Res. Suppl.* **89**, B525–B534.
- Dalrymple G. B. (1993) Preliminary report on $^{40}\text{Ar}/^{39}\text{Ar}$ incremental heating experiments on feldspar samples from the felsite unit, Geysers geothermal field, California. In *Active Geothermal Systems and Gold-Mercury Deposits in the Sonoma-Clear Lake Volcanic Fields, California*, (ed. J. J. Ryuba). Society of Economic Geologists Guidebook Series **16**, Littleton, Colorado pp. 131–140.
- Dalrymple G. B., Grove M., Lovera O. M., Harrison T. M., Hulen J. B., and Lanphere M. A. (1999) Age and thermal history of The Geysers plutonic complex (felsite unit), Geysers geothermal field, California; a $^{40}\text{Ar}/^{39}\text{Ar}$ and U-Pb study. *Earth Planet. Sci. Lett.* **30**, 285–298.
- Dickinson W. R. and Snyder W. S. (1979) Geometry of triple junctions related to San Andreas transform. *J. Geophys. Res.* **84**, 561–572.
- Donnelly-Nolan J. M., Hearn B. C. Jr., Curtis G. H., and Crake R. E. (1981) Geochronology and evolution of the Clear Lake volcanics. *U. S. Geol. Survey Prof. Pap.* **1141**, 47–60.
- Eberhart-Phillips D. (1986) Three-dimensional velocity structure in northern California Coast range from inversion of local earthquake arrival times. *Seism. Soc. Am. Bull.* **76**, 1025–1052.
- Fox Jr. F. K., Fleck R. J., Curtis G. H., and Meyer C. E. (1985) Implications of the northwestwardly younger age of the volcanic rocks of west-central California. *Geol. Soc. Am. Bull.* **96**, 647–654.
- Fukuoka T. and Kigoshi K. (1974) Discordant I_o-ages and the uranium and thorium distribution between zircon and host rocks. *Geochem. J.* **8**, 117–122.
- Futa K., Hedge C. E., Hearn Jr. B. C., and Donnelly-Nolan J. M. (1981) Strontium isotopes in the Clear Lake Volcanics. *U. S. Geol. Survey Prof. Pap.* **1141**, 61–66.
- Getty S. R. and DePaolo D. J. (1995) Quaternary geochronology using the U-Th-Pb method. *Geochim. Cosmochim. Acta* **5**, 3267–3272.
- Goes S., Govers R., Schwartz S. Y., and Furlong K. P. (1997) Three-dimensional thermal modeling for the Mendocino triple junction area. *Earth Planet. Sci. Lett.* **148**, 45–57.
- Green N. L. and Usdansky S. I. (1986) Ternary-feldspar mixing relations and thermobarometry. *Am. Mineralogist* **71**, 1100–1108.
- Gunderson R. P. (1991) Porosity of reservoir graywacke at the Geysers. In *Monograph on The Geysers Geothermal Field* (ed. C. Stone), Geothermal Research Council Special Report **17**, Davis, pp. 89–93.
- Halliday A. N., Mahood G. A., Holden P., Metz J. M., Dempster T. J., and Davidson J. P. (1989) Evidence for long residence times of rhyolitic magma in the Long Valley magmatic system; the isotopic record in precaldera lavas of Glass Mountain. *Earth Planet. Sci. Lett.* **94**, 274–290.
- Harrison T. M. and Watson E. B. (1983) Kinetics of zircon dissolution and zirconium diffusion in granitic melts of variable water content. *Contrib. Mineral. Petrol.* **84**, 66–72.
- Hazen R. M. and Finger L. W. (1979) Bulk modulus-volume relationship for cation-anion polyhedra. *J. Geophys. Res.* **B84**, 6723–6728.
- Hearn B. C., Donnelly-Nolan J. M., and Goff F. E. (1981) The Clear Lake Volcanics; tectonic setting and magma sources. *U. S. Geol. Survey Prof. Pap.* **1141**, 25–45.

- Hearn B. C., Donnelly-Nolan J. M., and Goff F. E. (1995) Geologic map and structure sections of the Clear Lake volcanics, Northern California. Scale 1:24,000. *U.S. Geol. Survey Map*, **I-2362**.
- Hildreth W. (1981) Gradients in silicic magma chamber: Implications for lithospheric magma chambers. *J. Geophys. Res.* **B86**, 10153–10192.
- Hinton R. W. and Upton B. G. J. (1991) The chemistry of zircon; variations within and between large crystals from syenite and alkali basalt xenoliths. *Geochim. Cosmochim. Acta* **55**, 3287–3302.
- Hulen J. B. and Nielson D. L. (1993) Interim report on geology of The Geysers felsite, Northwestern California. *Geothermal Res. Council Trans.* **17**, 249–258.
- Hulen J. B., Heizler M. T., Stimac J. A., Moore J. N., and Quick J. C. (1997) New constraints on the timing of magmatism, volcanism, and the onset of vapor-dominated conditions at The Geysers steam field, California. *Proceedings of the Twenty-Second Workshop on Geothermal Reservoir Engineering*, Stanford University, Stanford, California, pp. 75–81.
- Huppert H. E. and Sparks R. S. J. (1988) The generation of granitic magmas by intrusion of basalt into continental crust. *J. Petrol.* **29**, 599–624.
- Ihinger P. D., Hervig R. L., and McMillan P. F. (1994) Analytical methods for volatiles in glasses. In *Volatiles in Magmas* (ed. M. R. Carroll and J. R. Holloway), *Reviews in Mineralogy* **30**, Am. Mineral. Soc., Washington, pp. 67–121.
- Isherwood W. F. (1981) Geophysical overview of The Geysers. *U. S. Geol. Survey Prof. Pap.* **1141**, 83–96.
- Iyer H. M., Oppenheimer D. H., Hitchcock T., Roloff J. N., and Coakley J. M. (1981) Large teleseismic P-wave delays in The Geysers-Clear Lake geothermal area. *U. S. Geol. Survey Prof. Pap.* **1141**, 97–116.
- Johannes W. and Holtz F. (1996) *Petrogenesis and Experimental Petrology of Granitic Rocks*. Springer-Verlag, Berlin Heidelberg New York.
- Johnson C. M. and O'Neil J. R. (1984) Triple junction magmatism: A geochemical study of Neogene volcanic rocks in western California. *Earth Planet. Sci. Lett.* **71**, 242–262.
- Kennedy B. M. and Truesdell A. H. (1996) The Northwest Geysers high-temperature reservoir: Evidence for magmatic degassing and implications for the origin of The Geysers geothermal field. *Geothermics* **25**, 365–387.
- Lachenbruch A. H. and Sass J. H. (1980) Heat flow and energetics of the San Andreas fault zone. *J. Geophys. Res.* **B85**, 6185–6222.
- Levander A., Henstock T. J., Meltzer A. S., Beaudoin B. C., Trehu A. M., and Klemperer S. L. (1998) Fluids in the lower crust following Mendocino triple junction migration; active basaltic intrusion? *Geology* **26**, 171–174.
- Lejeune A.-M. and Richet P. (1995) Rheology of crystal-bearing silicate melts; an experimental study at high viscosities. *J. Geophys. Res.* **B100**, 4215–4229.
- Liu M. (1993) Thermal-volcanic evolution in the Northern California Coast Ranges. In *Active Geothermal Systems and Gold-Mercury Deposits in the Sonoma-Clear Lake Volcanic Fields, California* (ed. J. J. Rytuba), Society of Economic Geologists Guidebook Series **16**, Littleton, Colorado, pp. 26–37.
- Liu M. and Furlong K. P. (1992) Cenozoic volcanism in the California Coast Ranges: Numerical solutions. *J. Geophys. Res.* **B97**, 4941–4951.
- Lowenstern J. B., Persing H. M., Wooden J. L., Lanphere M., Donnelly-Nolan J., and Grove T. L. (2000) U-Th dating of single zircons from young granitoid xenoliths: New tools for understanding volcanic processes. *Earth Planet. Sci. Lett.* **183**, 291–302.
- Ludwig K. R. (1977) Effect of initial radioactive-daughter disequilibrium on U-Pb isotope apparent ages of young minerals. *J. Res. U. S. Geol. Survey* **5**, 663–667.
- Mahon K. (1996) The New 'York' regression: Application of an improved statistical method to geochemistry. *Int. Geol. Rev.* **38**, 293–303.
- Mankinen E. A., Donnelly J. M., and Grommé C. S. (1978) Geomagnetic polarity event recorded at 1.1 m.y. B.P. on Cobb Mountain, Clear Lake volcanic field, California. *Geology* **6**, 653–656.
- Mattinson J. M. (1973) Anomalous isotopic composition of lead in young zircons. *Carnegie Inst. Washington Year Book* **72**, 613–616.
- Mattinson J. M. (1988) Constraints on the timing of Franciscan metamorphism; geochronological approaches and their limitations. In *Rubey Colloquium on Metamorphism and Crustal Evolution of the Western United States – Rubey Volume 7* (ed. W. G. Ernst), Prentice-Hall, Englewood Cliffs, pp. 1023–1034.
- McDougall I. and Harrison T. M. (1999) *Geochronology and Thermochronology by the ⁴⁰Ar/³⁹Ar Method*. Oxford University Press, Oxford.
- McLaughlin R. J. (1981) Tectonic setting of pre-Tertiary rocks and its relation to geothermal resources in The Geysers-Clear Lake area. *U. S. Geol. Survey Prof. Pap.* **1141**, 301–316.
- McLaughlin R. J., Moore D. E., Sorg D. H., McKee E. H. (1983) Multiple episodes of hydrothermal circulation thermal metamorphism, and magma injection beneath the Geysers steam field, California. *Geological Society of America Abstracts with Programs* **15**, 417 (abstr.).
- Moore J. N., Adams M. C., and Anderson A. J. (2000) The fluid inclusion and mineralogic record of the transition from liquid- to vapor-dominated conditions in the Geysers geothermal system, California. *Econ. Geol.* **95**, 1719–1737.
- Norton D. L. and Hulen J. B. (2001) Preliminary numerical analysis of the magma-hydrothermal history of The Geysers geothermal system, California, USA. *Geothermics* **30**, 211–234.
- Paces J. B. and Miller J. D. (1993) Precise U-Pb ages of Duluth Complex and related mafic intrusions, northeastern Minnesota; geochronological insights to physical, petrogenetic, paleomagnetic, and tectonomagnetic processes associated with the 1.1 Ga Midcontinent Rift System. *J. Geophys. Res.* **98**, 13997–14013.
- Pearce N. J. G., Perkins W. T., Westgate J. A., Gorton M. P., Jackson S. E., Neal C. R., and Chery S. P. (1997) Compilation of new and published major and trace element data for NIST SRM 610 and NIST SRM 612 glass reference materials. *Geostand. Newslett.* **21**, 115–144.
- Pichavant M. (1981) An experimental study of the effect of boron on a water saturated haplogranite at 1 kbar vapour pressure. *Contrib. Mineral. Petrol.* **76**, 430–439.
- Reid M. R. and Coath C. D. (2000) In situ U-Pb ages of zircons from the Bishop Tuff; no evidence for long crystal residence times. *Geology* **28**, 443–446.
- Reid M. R., Coath C. D., Harrison T. M., and McKeegan K. D. (1997) Prolonged residence times for the youngest rhyolites associated with Long Valley Caldera; ²³⁰Th-²³⁸U ion microprobe dating of young zircons. *Earth Planet. Sci. Lett.* **150**, 27–39.
- Renne P. R., Swisher C. C., Deino A. L., Karner D. B., Owens T. L., and DePaolo D. J. (1998) Intercalibration of standards, absolute ages and uncertainties in ⁴⁰Ar/³⁹Ar dating. *Chem. Geol.* **145**, 117–152.
- Ryerson F. J., Weed H. C., and Piwinski A. J. (1988) Rheology of subliquidus magmas; 1. Picritic compositions. *J. Geophys. Res.* **B93**, 3421–3436.
- Sambridge M. S. and Compston W. (1994) Mixture modeling of multi-component data sets with application to ion probe zircon ages. *Earth Planet. Sci. Lett.* **128**, 373–390.
- Sañudo-Wilhelmy S. A. and Flegal A. R. (1994) Temporal variations in lead concentrations and isotopic composition in the Southern California Bight. *Geochim. Cosmochim. Acta* **58**, 3315–3320.
- Schärer U. (1984) The effect of initial ²³⁰Th disequilibrium on young U-Pb ages: The Makalu case, Himalaya. *Earth Planet. Sci. Lett.* **67**, 191–204.
- Schmitt A. K., Grove M., Harrison T. M., Lovera O., Hulen J. B., Walters M. (2002) The Geysers-Cobb Mountain Magma System, California. (Part 2): Timescales of pluton emplacement and implications for its thermal history. *Geochim. Cosmochim. Acta* **67**, 3343–3458.
- Schriener Jr. A. and Suemnicht G. A. (1981) Subsurface intrusive rocks at The Geysers geothermal area, California. In *Proceedings of the Symposium on Mineral Deposits of the Pacific Northwest* (ed. M. L. Silberman, C. W. Field, and A. L. Berry), *U. S. Geological Survey Open-file Rep.* **81-355**, 295–302.
- Shackleton N. J., Berger A., and Peltier W. A. (1990) An alternative astronomical calibration of the lower Pleistocene timescale based on ODP Site 677. *Trans. Royal Soc. Edinburgh Earth Sci.* **81**, 251–261.
- Smith R. L. (1979) Ash-flow magmatism. *Geol. Soc. Am. Special Paper* **180**, 5–28.

- Stanley W. D. and Blakely R. J. (1995) The Geysers-Clear Lake geothermal area, California – an updated geophysical perspective of heat sources. *Geothermics* **24**, 187–221.
- Stanley W. D., Benz H. M., Walters M. A., Villaseñor A., and Rodriguez B. D. (1998) Tectonic controls on magmatism in The Geysers-Clear Lake region: Evidence from new geophysical models. *Geol. Soc. Am. Bull.* **110**, 1193–1207.
- Stimac J. A., Goff F. A., and Wohletz K. (2001) Thermal modeling of the Clear Lake magmatic-hydrothermal system, California, USA. *Geothermics* **30**, 349–390.
- Stix J. and Layne G. D. (1996) Gas saturation and evolution of volatile and light lithophile elements in the Bandelier magma chamber between two caldera-forming eruptions. *J. Geophys. Res.* **101**, 25181–25196.
- Turrin B. D., Donnelly-Nolan J. M., and Hearn Jr. B. C. (1994) $^{40}\text{Ar}/^{39}\text{Ar}$ ages from the rhyolite of Alder Creek, California: Age of the Cobb Mountain normal-polarity subchron revisited. *Geology* **22**, 251–254.
- Vazquez J. A. and Reid M. R. (2002) Time scales of magma storage and differentiation of voluminous high-silica rhyolites at Yellowstone caldera, Wyoming. *Contrib. Mineral. Petrol.* **144**, 274–285.
- Walters M. A. and Combs J. (1992) Heat flow in The Geysers-Clear Lake Geothermal area of northern California, USA. In *Monograph on The Geysers Geothermal Field* (ed. C. Stone), Geothermal Research Council Special Report **17**, Davis, pp. 43–53.
- Watson E. B. and Harrison T. M. (1983) Zircon saturation revisited; temperature and composition effects in a variety of crustal magma types. *Earth Planet. Sci. Lett.* **64**, 295–304.
- Watson E. B., Cherniak D. J., Hancher J. M., Harrison T. M., and Wark D. A. (1997) The incorporation of Pb into zircon. *Chem. Geol.* **141**, 19–31.
- Webster J. D. and Holloway J. R. (1988) Experimental constraints on the partitioning of Cl between topaz rhyolite melt and H_2O and $\text{H}_2\text{O}+\text{CO}_2$ fluids; new implications for granitic differentiation and ore deposition. *Geochim. Cosmochim. Acta* **52**, 2091–2105.
- Wendt I. and Carl C. (1985) U/Pb dating of discordant 0.1 Ma old secondary U minerals. *Earth Planet. Sci. Lett.* **73**, 278–284.
- Wiedenbeck M., Alle P., Corfu F., Griffin W. L., Meier M., Oberli F., Von Quadt A., Roddick J. C., and Spiegel W. (1995) Three natural zircon standards for U-Th-Pb, Lu-Hf, trace element and REE analyses. *Geostandards Newslett.* **91**, 1–23.
- Williams C. F., Galanis Jr. S. P., Moses Jr. T. H., and Grubb F. V. (1993) Heat-flow studies in the Northwest Geysers geothermal field, California. *Geothermal Research Council Transactions* **17**, 281–288.
- Winick J. A., McIntosh W. C., and Dunbar N. W. (2001) Melt-inclusion-hosted excess ^{40}Ar in quartz crystals of the Bishop and Bandelier magma systems. *Geology* **29**, 275–278.
- Zhang Y., Stolper E. M., and Wasserburg G. J. (1999) Diffusion of water in rhyolitic glasses. *Geochim. Cosmochim. Acta* **55**, 441–456.